



24 **Abstract**

25           The Lightning Imaging Sensor (LIS) was launched to the International Space Station (ISS)  
26 in February 2017, detecting optical signatures of lightning with storm-scale horizontal  
27 resolution during both day and night. ISS LIS data are available beginning 1 March 2017.  
28 Millisecond timing allows detailed intercalibration and validation with other spaceborne and  
29 ground-based lightning sensors. Initial comparisons with those other sensors suggest flash  
30 detection efficiency around 60%, false alarm rate under 5%, timing accuracy better than 2 ms,  
31 and horizontal location accuracy around 3 km. The spatially uniform flash detection capability  
32 of ISS LIS from low-Earth orbit allows assessment of spatially varying flash detection efficiency  
33 for other sensors and networks, particularly the Geostationary Lightning Mappers. ISS LIS  
34 provides research data suitable for investigations of lightning physics, climatology,  
35 thunderstorm processes, and atmospheric composition, as well as realtime lightning data for  
36 operational forecasting and aviation weather interests. ISS LIS enables enrichment and  
37 extension of the long-term global climatology of lightning from space, in particular to higher  
38 latitudes ( $\pm 55^\circ$ ) than was recently possible. The global spatial distribution of lightning from ISS  
39 LIS is broadly similar to previous datasets, and globally averaged seasonal/annual flash rates  
40 agree within 5-10% as well. The expected land/ocean contrast in the diurnal variability of global  
41 lightning is also observed.

42 **Plain Language Summary**

43           The Lightning Imaging Sensor on the International Space Station (ISS LIS) has been  
44 operating on-orbit since February 2017. The instrument has met all of its major science  
45 objectives, including detecting lightning day and night, identifying the specific locations within  
46 storms that are producing lightning, millisecond timing accuracy, and high probability of  
47 detecting lightning. The instrument also measures energy emitted by lightning, provides  
48 background images of storms and their surroundings, and delivers realtime lightning data. This  
49 has enabled enrichment and extension of the long-term global climatology of lightning from  
50 space, in particular to higher latitudes (+/- 55 degrees) than was recently possible. In addition,  
51 the instrument is serving as a standard for comparison to other spaceborne lightning sensors,  
52 such as the Geostationary Lightning Mapper (GLM). The realtime data from ISS LIS have  
53 enabled new applications for the benefit of the public, including weather forecasting and public  
54 safety. Finally, ISS LIS - in conjunction with other satellite instruments - is providing  
55 opportunities for new scientific study in areas such as lightning physics, thunderstorm  
56 processes, and atmospheric composition.

57 **Key Points**

- 58 1. The Lightning Imaging Sensor (LIS) has been operational on the International Space  
59 Station (ISS) since February 2017.
- 60 2. ISS LIS provides storm-scale resolution (4-km) and millisecond timing of global lightning  
61 with high uniform detection efficiency (~60%).
- 62 3. The 3-year global lightning climatology is consistent with previous studies (within 5-  
63 10%), while extending results to higher latitudes.

64

65 **1. Introduction**

66 Lightning is a spectacular and direct response to strong thundercloud electric fields,  
67 which in turn are generated by intense atmospheric moist convection and (normally) the onset  
68 of active precipitation processes involving ice particles [Saunders, 2008]. Since lightning is  
69 inherently coupled to storm microphysics and dynamics, it can be used as a valuable tool to  
70 remotely probe the developmental state, severity, and evolution of thunderstorms and  
71 thunderstorm complexes [e.g., Yoshida et al., 2017; Darden et al., 2009 and references therein].  
72 Because a lightning discharge produces lightning nitrogen oxides (LNO<sub>x</sub>), which in turn affect  
73 greenhouse gas concentrations (such as ozone), lightning also serves as a key indicator for  
74 monitoring long-term climate change, and plays an important role in affecting air quality  
75 forecasts [Koshak et al., 2014a,b; Koshak et al., 2015]. Overall, lightning provides useful  
76 information about a variety of atmospheric processes and offers vital scientific insight across a  
77 broad range of disciplines, such as weather, climate, atmospheric chemistry, and lightning  
78 physics.

79 The Lightning Imaging Sensor (LIS) on the International Space Station (ISS) plays a special  
80 role in improving our understanding of these complex interrelationships. The optically based  
81 lightning detection instrument was launched to the ISS in February of 2017, and has  
82 successfully operated with limited downtime since. The ISS, which is in a low-Earth orbit (LEO)  
83 inclined near 55°, has been increasingly used as a host for a number of Earth-observing  
84 instruments due to its accessibility; ample space, power, and data bandwidth; and ability to  
85 precess through the diurnal cycle.

86           This paper will describe the ISS LIS instrument and its data products, document key  
87 performance metrics and science results from its first three years on orbit, discuss applications  
88 enabled by near-realtime ISS LIS data, and point toward new opportunities for cross-platform  
89 science that are enabled by using ISS LIS in conjunction with other Earth-observing instruments.

90

## 91 **2. ISS LIS instrument and data structure**

92           The ISS LIS instrument heritage spans multiple decades. The National Aeronautics and  
93 Space Administration (NASA) Marshall Space Flight Center (MSFC) - along with support from  
94 other science, academic, and commercial partners - developed a unique space-based lightning  
95 detection instrument, the Optical Transient Detector (OTD). The instrument design concept  
96 began in earnest in the 1980s with high-altitude aircraft measurements of cloud-top lightning  
97 optical signatures [*Christian et al., 1983*]. These measurements helped determine optimal  
98 space-based instrument requirements (e.g., what sensitivity would be required to detect  
99 lightning under both day and night conditions). The OTD was then engineered from these  
100 requirements in the early 1990s, and was launched aboard the MicroLab-1 satellite in 1995  
101 from Vandenberg Air Force Base. It provided the first global-scale lightning climatology for its  
102 operational lifetime (1995-2000) [*Christian et al., 2003*].

103           The OTD was essentially a prototype design for the LIS concept developed as part of the  
104 NASA Earth Observing System (EOS). The LIS was selected as an EOS instrument to fly on both a  
105 polar platform and the ISS, then known as Space Station Freedom. However, all the EOS  
106 instruments for ISS were descoped within about a year because NASA wanted to focus primarily  
107 on getting the ISS built. Later, LIS was moved to the Tropical Rainfall Measuring Mission

108 (TRMM) instrument complement because it had strong synergies with the core TRMM science  
109 instruments [Kummerow *et al.*, 1998]. TRMM LIS was launched in November of 1997 and ended  
110 its mission with the deorbiting of the TRMM satellite in April of 2015 (i.e., a very successful 17+  
111 years of operational lifetime).

112 Building on this long and dynamic heritage, the flight spare instrument for TRMM LIS  
113 was adapted to work on the ISS platform, resulting in ISS LIS. ISS LIS was part of the 5<sup>th</sup> Space  
114 Test Program - Houston mission (STP-H5), which is sponsored by the US Department of Defense  
115 (DoD). ISS LIS is currently located on the Express Logistics Carrier 1 (ELC-1) module of the ISS  
116 (Fig. 1).

117 Relative to TRMM LIS, ISS LIS extends the program of record for global coverage of low-  
118 latitude lightning ( $\pm 38^\circ$ ). Relative to OTD, ISS LIS extends the program of record for higher  
119 latitude lightning (up to  $\pm 55^\circ$ ). And relative to geostationary lightning sensors, ISS LIS enables  
120 fully global coverage as well as cross-platform validation. Thus, ISS LIS is a unique Earth-  
121 observing instrument that provides near-realtime observations of lightning, including global  
122 coverage to high latitudes (observing an estimated 98% of all global lightning) throughout the  
123 diurnal and seasonal cycles.

124 In terms of NASA EOS Data and Information System (EOSDIS) Data Processing Levels, the  
125 ISS LIS science data are Level 2 (i.e., derived geophysical variable), while the background data  
126 are Level 1B (i.e., reconstructed instrument data processed to sensor units). The data are  
127 available in the TRMM LIS heritage Hierarchical Data Format Version 4 (HDF4) as well as the  
128 modern Network Common Data Format Version 4 (netCDF4), with corresponding browse  
129 images in Graphics Interchange Format (GIF).

130 ISS LIS products are produced and distributed by the NASA Global Hydrology Resource  
131 Center (GHRC) Distributed Active Archive Center (DAAC; Figs. 1 and 2) and can be discovered  
132 via the NASA Earthdata Search tool [*Earthdata*, 2020], the GHRC Hydrology Data Search Tool  
133 [*HyDRO*, 2020], and the GHRC website for ISS LIS [*ISS LIS*, 2020].

134 The LIS measurement concept, which is based on time-differenced geolocated images at  
135 777.4-nm wavelength [*Christian et al.*, 1989], an oxygen-absorption line that enables detection  
136 of lightning signals at cloud top during both day and night, was recently adapted to work from  
137 geostationary orbit [*Goodman et al.*, 2013; *Rudlosky et al.*, 2018]. This enables continuous  
138 spaceborne lightning observations over a hemispheric field of view (FOV).

139

### 140 **3. Results**

141 ISS LIS has operated successfully for more than three years. Among many other  
142 accomplishments, all major science objectives for the instrument have been achieved. In  
143 addition, a climatology of global lightning has been produced and compared to similar datasets.  
144 Cross-platform validation against other datasets has been performed, and new cross-platform  
145 science applications are being developed. Finally, a diverse user community is developing due  
146 to applications enabled by near-realtime ISS LIS data. These results are summarized in the  
147 subsections below.

148

#### 149 *3.1 Achievement of major science objectives*

150 A primary and fundamental accomplishment in the past 3 years has been the successful  
151 achievement of all major science objectives of the instrument. These objectives include the

152 detection of lightning during day and night, with storm-scale spatial resolution, millisecond  
153 timing, and high flash detection efficiency without a land/ocean bias. ISS LIS was designed to  
154 measure radiant energy and provide background images/intensity, and its deployment on the  
155 ISS enables the delivery of realtime lightning data. These objectives were achieved by  
156 successfully meeting the following instrument/platform requirements.

157

### 158 3.1.1 Successfully characterize the instrument's field of view (FOV)

159 The ISS LIS instrument has a  $78.5^\circ \times 78.5^\circ$  rectangular FOV imaged on a 128 x 128 pixel  
160 charge coupled device (CCD). At 400-km altitude this provides "storm-scale" pixel resolution  
161 (nadir) of  $\sim 4$  km (and 50% larger at off-nadir boundaries), which is similar to TRMM LIS after its  
162 orbit boost in 2001. Obscuration of the FOV by ISS solar panels and radiator that periodically  
163 pass through the FOV was quantified. Worst-case mean and peak obscuration is 4% and 12.5%,  
164 respectively. Since ISS is a moving platform, small obstructions in the FOV will only lower view-  
165 time of a point on the ground (e.g., storm) momentarily, so there is no impact to science  
166 provided the view times are appropriately adjusted. Current version 1 ISS LIS data likely have a  
167 slight, artificially reduced ( $\sim 1$ -2%) detection efficiency (DE) due to overestimates of viewing  
168 times. FOV analysis remains an ongoing process, and improved viewing time estimates are  
169 expected in version 2 ISS LIS data.

170

### 171 3.1.2 Mitigate solar glare/glint, and control the thermal and contamination environments

172 Reflection of direct sunlight into the sensor will not damage LIS, but sufficient glint  
173 signal could momentarily "blind" LIS by filling its first-in/first-out (FIFO) buffer. Pre-launch,

174 Manipulator Analysis Graphics and Interactive Kinematics (MAGIK) analysis was performed by  
175 NASA Johnson Space Center (JSC) to assess potential glare/glint and its impact. No glare spots  
176 or rapidly changing illumination were detected from either the solar panels or radiator. Images  
177 obtained from nadir-viewing cameras in STP-H4 (another STP mission located close to ISS LIS)  
178 qualitatively corroborate this result. Analysis of numerous other ISS images and videos also  
179 supported this inference (not shown).

180         During mission development, STP-H5 and LIS engineers examined both survival (during  
181 transfer) and temperature exceedance during operation. It was found that on-orbit  
182 temperatures remained within acceptable limits. Realtime housekeeping data from ISS LIS,  
183 including relevant temperatures, are gathered and posted to an internal website. These data  
184 are regularly monitored to ensure nominal instrument performance.

185         Modeling analysis was conducted for the molecular contamination effects on the LIS  
186 window transmission at 777.4 nm. The modeling was based on previous flight data from  
187 materials exposed in the ISS environment and estimations of outgassing rates in that  
188 environment for the mission duration of 3 years. Values were taken from baseline external  
189 contamination assessments collected during pre-launch testing. Worst case scenario showed  
190 only a 5% decrease in absolute transmission over 3 years due to typical contaminants. Note that  
191 the nearly identical TRMM LIS instrument showed very limited performance degradation over  
192 its 17-year life span [Buechler *et al.*, 2014].

193

#### 194 3.1.4 Laboratory calibration

195           The laboratory calibration of TRMM LIS is discussed in detail in *Koshak et al.* [2000], and  
196 this was the same calibration approach applied to the spare LIS unit (i.e., ISS LIS). The  
197 calibration consisted of four main efforts: (1) a static response test, a (2) transient response  
198 test, (3) a spectral test, and (4) an FOV test. Additional elements of the calibration pertinent to  
199 LIS performance characteristics are discussed in *Boccippio et al.* [2002].

200           The calibration tests, which are referred to here as the original calibration (OC), were  
201 carried out on both the original TRMM LIS and the spare unit (the future ISS LIS) in the summer  
202 of 1997. TRMM LIS was subsequently launched to orbit, while the spare unit was stored in a  
203 safe box in an environmentally controlled facility for many years, until it was integrated on STP-  
204 H5. In the summer of 2014 and prior to the integration on STP-H5, a retest calibration (RC) was  
205 performed on the spare unit to evaluate if there were any significant changes in the OC given  
206 the many years that the unit was in storage. The RC instrumentation and procedures employed  
207 were made as similar as possible to that employed in the OC, but unfortunately the OC and RC  
208 methodologies were not identical.

209           A brief overview of the OC tests applied to both the TRMM LIS and ISS LIS are provided  
210 below:

- 211       • **Static Response Test:** The OC static response test provided the linear response of each  
212 pixel, and hence also quantified uniformity across the charge coupled device (CCD)  
213 array. It employed an 8-inch integrating sphere calibration standard. The sphere lamp  
214 source emitted a static radiance that was nearly isotropic and uniform over the 2-inch  
215 diameter exit port (source stability at 3000 K color temperature was specified at  $\pm 0.5\%$   
216 over a 1-hr duration, and  $\pm 2.0\%$  over 100 hr). The radiance was continuously adjustable

217 over a range of five orders of magnitude without changing the color temperature. Since  
218 the sphere output could not fill the sensor FOV, a motorized positioning system  
219 (containing precision Newport/Klinger rotation stages) was used to yaw and pitch the  
220 sensor head to effect full FOV coverage.

221 • **Transient Response Test:** The purpose of the OC transient response test was to  
222 determine the transient response of the sensor to optical pulses of various integrated  
223 energies, against several different levels of steady-state background radiance, and for  
224 several different pixels across the CCD array. Pulse energy was varied by varying the  
225 pulse duration within a 2-ms LIS frame. The primary component of the test system was a  
226 2-inch integrating sphere containing a near-infrared light emitting diode (LED) and a  
227 small quartz tungsten halogen (QTH) lamp. The LED was mounted behind a pinhole in  
228 the far surface of the sphere. Background radiance levels were adjusted by a variable  
229 aperture in the lamp input port, thus maintaining a constant color temperature.

230 • **Spectral Response Test:** The OC spectral test employed a high-resolution grating  
231 monochromator (500-mm focal length, f/5 aperture, and 0.1-nm resolution) as the  
232 primary component. The attached source module contained a QTH lamp and a krypton  
233 rare gas discharge lamp as a wavelength reference. The monochromator output was fed  
234 through a fiber-optic cable whose output was approximately collimated by a small off-  
235 axis paraboloid mirror. By scanning in wavelength, the spectral test determined the  
236 sensor end-to-end relative spectral response. This test covered only the wavelength  
237 region near and within the passband of the narrowband interference filter.

238 • **FOV Test:** The FOV test in the OC employed a 9-inch diameter, off-axis paraboloid mirror  
239 and an infrared LED. The LED was used to illuminate a total of 31 pixels that were evenly  
240 spaced across the CCD, and the associated source incidence angles for each pixel was  
241 computed. The LED incidence angles to the lens could be viewed equivalently as  
242 lightning source angles. The geometrical mappings were mathematically unique and  
243 were used to build a lens transfer function (i.e., boresight angle vs. pixel distance from  
244 center of the CCD). These results are fundamental to the process of geolocating  
245 lightning. The overall sensor FOV (approximately  $78.5^\circ \times 78.5^\circ$ ) was determined by  
246 simply illuminating pixels on the CCD perimeter.

247 As mentioned previously, the RC methodology and equipment were not identical to the  
248 OC. In the fall of 2013, prior to beginning the RC, it was deemed necessary to upgrade much of  
249 the equipment employed in the OC, since these were out of date and were no longer  
250 compatible with current technology. For the static response test, two integrating sphere  
251 systems were procured. The first was a 12-inch sphere with a large aperture which was  
252 intended to allow uniform illumination of a larger portion of each quadrant of the ISS LIS  
253 instrument. The second was a 6-inch sphere that was comparable but not the same size as the  
254 8-inch sphere used in the OC. This second sphere was acquired for the purposes of transient  
255 testing, as it had a removable port in the back for attaching an LED.

256 Ultimately the 12-inch sphere was deemed unusable for the static response test  
257 because the large opening allowed for “hotspots” where the luminosity was greater  
258 surrounding the tungsten bulbs. The 6-inch sphere worked for testing the static response of the  
259 instrument; however, it only covered a fraction of each of the quadrants. After comparing the

260 results with the legacy calibration, it was noticed that there was a form factor difference, so the  
261 legacy 8-inch sphere was then used to determine if the values were still the same as the legacy  
262 calibration. Using the legacy sphere as a one-to-one comparison with the previous calibration  
263 was a success.

264 Use of the 6-inch sphere for transient testing was originally the plan; however, after  
265 inserting the newly painted LED insert there were noticeable differentials in the reflectivity of  
266 the new insert, especially around the edges. It was decided to use the LED as the source for the  
267 backgrounds for each pixel and then on top of that send the pre-programmed transient signal.  
268 This allowed for a very controllable and fluid process for the transient calibration.

269 For the spectral test, the grating monochromator used in the OC could no longer be  
270 used because the controller was no longer available, and the connections were obsolete.  
271 Instead, a new monochromator was employed for the RC. The FOV test for the RC was  
272 performed in much the same way as in the OC, and the results were essentially identical.

273 ISS LIS alignment measurements were conducted in the RC. The alignment  
274 measurements were obtained by illuminating different sides of a mirror-faced alignment cube  
275 (attached to the outside of the LIS sensor head assembly) with a theodolite; this allowed  
276 determination of the overall rigid alignment of the LIS lens/CCD systems with the STP-H5  
277 module and ISS platform.

278 While the RC procedure was acceptable, it was not optimal. The intent of the RC was to  
279 ensure that nothing significantly changed with the instrument during the years in storage. For  
280 expediency, and because the RC results showed no significant changes from the OC results for

281 TRMM LIS (Fig. 3), the OC results for the TRMM LIS were applied in the ISS LIS processing code,  
282 which produces the version 1 dataset available at the GHRC.

283           However, a plan is being implemented to replace the TRMM LIS OC results in the ISS LIS  
284 processing code with the ISS LIS OC results, since identical procedures could not be followed  
285 due to the passage of time. In particular, the RC static response test was incomplete because it  
286 did not cover all pixels in the CCD array; it only illuminated a small circular portion in the center  
287 of each quadrant. This leaves some lingering calibration uncertainties in the version 1 ISS LIS  
288 dataset. The ISS LIS science team is working to retrieve the digital OC calibration data for the  
289 spare unit, and before updating the ISS LIS processing code the ISS OC and RC results will be  
290 compared in detail, as well as with the OC results for TRMM LIS. Based on initial analysis, an  
291 improvement of 2-5% in key instrument performance parameters (e.g., flash detection  
292 efficiency, flash false alarm rate, geolocation accuracy, and optical amplitudes) is expected after  
293 a future switch to the ISS LIS OC.

294

### 295 3.1.5 Quantify timing, geolocation/pointing, detection efficiency, and false alarm rate

296           Like TRMM LIS, ISS LIS has a frame rate of  $500 \text{ s}^{-1}$ . This implies a native 2-ms timing  
297 precision. The actual on-orbit timing *accuracy* of ISS LIS was determined by comparison against  
298 multiple ground-based and spaceborne reference datasets. The ground-based reference  
299 datasets were the EarthNetworks Global Lightning Network (ENGLN), which operates wideband  
300 sensors (1 Hz to 12 MHz), and the Vaisala Global Lightning Dataset 360 (GLD360), which detects  
301 waveforms in the very low frequency range (VLF;  $\sim 500 \text{ Hz}$  to  $\sim 50 \text{ kHz}$ ). Both of these are global  
302 datasets. The spaceborne reference datasets were the Geostationary Operational

303 Environmental Satellite (GOES) 16 and 17 Geostationary Lightning Mappers (GLM-16 and GLM-  
304 17) [Goodman *et al.*, 2013, Rudlosky *et al.*, 2018]. GLM is built on the LIS/OTD optical detection  
305 heritage and is sensitive to both IC and CG lightning.

306 The timing data as initially received from ISS exhibited offsets up to  $\pm 1$  s with respect to  
307 the reference data, with an alternating drift pattern that cycled approximately every 9 days.  
308 This drift was accurately characterized based on careful analysis. On the basis of this, timing  
309 correction variables, and an additional constant offset, were applied to produce the current  
310 timing accuracy (Fig. 4 left).

311 After correction, ISS LIS has modal temporal offset of +1 ms, or approximately one-half  
312 the LIS frame duration, when compared with GLM-16/17 (Fig. 4 left). The standard deviation in  
313 the offset is less than 2 ms in either direction, compared to GLM-16/17. This comparison was  
314 based on group timings between ISS LIS and the GLM datasets. Relative to the ground-based  
315 reference datasets, there is zero modal offset, and the standard deviation is also below 2 ms.  
316 Thus, after correction for the ISS timing errors, the ISS LIS timing accuracy is less than the native  
317 timing precision of the instrument itself (2 ms).

318 ISS LIS geolocation accuracy was analyzed through a coordinate system transform  
319 technique that allowed LIS location errors with respect to the reference data to be displayed in  
320 the native LIS field-of-view. This analysis revealed that the ISS navigation variables used for LIS  
321 geolocation vary systematically during each orbit, creating location errors of up to 25 km. The  
322 ISS LIS team worked diligently to troubleshoot the initial issues with geolocation (and timing), as  
323 these posed complex interconnected problems that took focused analysis, data deep-dives, and  
324 skilled interpretations to resolve.

325           An iterative tuning process resolved these initial problems and produced corrected  
326 geolocation data and the current analysis of ISS LIS spatial accuracy (Fig. 4 right). Relative to  
327 GLM-16/17, corrected ISS LIS spatial offsets are almost entirely less than 10 km, with the vast  
328 majority below 5 km. Offsets relative to ENGLN and GLD360 are distributed more broadly, but  
329 for each of the spaceborne and ground-based reference datasets the modal offset is  
330 approximately 2-3 km. This means that ISS LIS has achieved sub-pixel (< 4 km) location  
331 accuracy.

332           Timing, location, flash DE, and false alarm rate (FAR) have been stable during most of  
333 the mission to date. Figure 5 shows the time series of these parameters through early 2020. ISS  
334 LIS temporal accuracy offset shifted by about 1 ms on 16 December 2018, such that LIS now  
335 slightly leads the reference data (Fig. 5 top). A few larger deviations occurred during two  
336 periods in early 2019, related to atypical ISS maneuvers. However, in most circumstances the  
337 absolute magnitude of the offsets remain less than 2 ms. LIS geolocation accuracy also has been  
338 stable throughout the mission (Fig. 5 middle), with the peak offset normally less than 5 km. The  
339 detection performance of ISS LIS is also stable over time (Fig. 5 bottom), aside from the known  
340 deviations in early 2019 mentioned above. The flash DE is stable with respect to each of the  
341 reference datasets (64% relative to GLM, and 56-57% relative to ENGLN/GLD360), and the FAR,  
342 calculated over the Americas domain where the greatest quantity and best quality reference  
343 data are available, is under 5% on average.

344

### 345 *3.2 Lightning climatology*

346           The ISS LIS lightning climatology has been completed for the first three years of data  
347 (March 2017 - Feb 2020; Fig. 6a). Within  $\pm 38^\circ$  latitude, these results are broadly similar to the  
348 more than 13-year (after orbit boost; September 2001 - December 2014) TRMM LIS climatology  
349 (Fig. 6b). During this period, TRMM had a nominal orbit altitude of 402.5 km - very similar to  
350 the ISS orbit altitude range of 400-405 km. (The TRMM pre-boost orbit altitude was  
351 substantially lower, at 350 km, and thus is not considered here to keep the comparison more  
352 direct.)

353           Because ISS LIS has a shorter period of record, the lightning density maps are not as  
354 smooth despite the  $0.5^\circ$  gridding (Fig. 6a). However, notable hotspots [Albrecht *et al.*, 2016]  
355 from the TRMM LIS climatology (Fig. 6b), such as central Africa, Paraguay/northern  
356 Argentina/Rio Grande do Sul (Brazil), Lake Maracaibo (Venezuela), the Himalayas/Indian  
357 Subcontinent, and the Maritime Continent stand out, and feature comparable flash rates  
358 between ISS and TRMM LIS. For example, peak flash rates over central Africa exceed  $80 \text{ km}^{-2} \text{ yr}^{-1}$   
359 <sup>1</sup> in both datasets. The well-known stark contrast between land and ocean lightning flash rates  
360 also stands out in both plots, as do the coastal enhancements in lightning over the Gulf Stream,  
361 near west Africa, the Caribbean and near Central America, near southeastern Brazil, the Bay of  
362 Bengal, etc. ISS LIS also has been able to observe the small enhancements in lightning over the  
363 open Pacific, between  $\pm 30^\circ$  latitude, west of  $-120^\circ$  (south Pacific) and  $-150^\circ$  (north Pacific)  
364 longitude (including the Intertropical Convergence Zone, ITCZ). This is similar to TRMM LIS (Fig.  
365 6b), but the patterns are more diffuse due to fewer samples.

366           In the global aggregate, lightning flash rates (between  $\pm 38^\circ$  latitude) are comparable  
367 between ISS LIS and TRMM LIS (Fig. 7). Both datasets show globally averaged flash rate ranging

368 between 25 and 55 s<sup>-1</sup>. This, along with Fig. 6, demonstrates that ISS LIS is making  
369 fundamentally similar observations to TRMM LIS, and thus is capable of extending the TRMM  
370 LIS dataset over the tropics and subtropics for a longer time period.

371 ISS LIS enables coverage of higher latitudes ( $\pm 55^\circ$ ) compared to TRMM LIS ( $\pm 38^\circ$ ). This  
372 allows more complete viewing of the Great Plains of the United States (US), which features  
373 flash rates  $\sim 30 \text{ km}^{-2} \text{ yr}^{-1}$  extending as far north as the border with Canada (Fig. 6a). The  
374 improved coverage of the continental US is a particularly important advantage of ISS LIS,  
375 because this coverage allows for a more robust examination of lightning/climate relationships  
376 within ongoing National Climate Assessment (NCA) studies [Koshak, 2017]. Another mid-  
377 latitude hot spot over Manchuria is also observed by ISS LIS, and the coastal enhancement of  
378 lightning near eastern South America is seen to extend further south. ISS LIS also provides  
379 coverage of most of Europe, including the lightning enhancement near the Alps. Lightning  
380 enhancement over Turkey is observed by ISS LIS.

381 The combined TRMM LIS and OTD dataset [Cecil *et al.*, 2014] provides a useful point of  
382 comparison for ISS LIS. OTD was in LEO orbit at 70° inclination and 740-km altitude [Christian *et*  
383 *al.*, 2003], so it provided coverage at higher latitudes than ISS LIS, but with reduced spatial  
384 resolution and geolocation accuracy. Table 1 shows a comparison of globally averaged flash  
385 rates from ISS LIS relative to the OTD and TRMM LIS climatology published by Cecil *et al.* [2014].  
386 ISS LIS is measuring slightly lower flash rates, but the numbers are within 5-10% of the previous  
387 climatology, which is well within the magnitude of expected offset from the slight viewing time  
388 overestimates in version 1 ISS LIS data (Section 3.1.1), as well as interannual variability (e.g., Fig.  
389 7). In addition, there is significant lightning northward of 55° during boreal summer due to

390 northern hemisphere land masses; thus, even with improved viewing time estimates, ISS LIS is  
391 not expected to provide global flash rates as high as *Cecil et al.* [2014] during June-August.

392 Relative to *Cecil et al.* [2014], ISS LIS has observed potentially higher flash rates in  
393 notable mid-latitude areas - such as Turkey and the Middle East, southern Canada, Manchuria,  
394 Europe and Northern Africa (Fig. 6a). However, caution in interpreting the 3-year ISS LIS dataset  
395 is required, since the relative impacts of individual storms may be influencing these differences.  
396 Integration of ISS LIS observations into the full LIS/OTD gridded dataset, which will enable  
397 detailed quantitative comparisons for individual regions, is planned for a future study.

398 The seasonal distribution of lightning from ISS LIS also follows expectations established  
399 by previous global climatologies (Fig. 8). Globally, lightning is maximized during June-August  
400 (Fig. 8b); however, both March-May and September-November also have significant activity  
401 (Fig. 8a, c). Notably, in boreal autumn the northern Great Plains of the US can remain active,  
402 even as similar latitude locations in Europe, for example, see a substantial decrease from the  
403 summertime peak (Fig. 8c). The Manchuria lightning peak is primarily a boreal summertime  
404 phenomenon, with a significant decrease in both spring and fall. Lightning in the Middle East is  
405 most prevalent during boreal spring and fall, while Turkey reaches its maximum in summer.  
406 Boreal winter leads to a significant reduction in northern hemisphere lightning (Fig. 8d);  
407 however, there are noticeable hot spots remaining in the US Gulf Coast. The lightning peak near  
408 Paraguay is most distinctive during austral spring (Fig. 8c).

409 Globally averaged diurnal variability of lightning (Fig. 9) follows the typical patterns  
410 observed in previous climatologies [*Virts et al.*, 2013; *Blakeslee et al.*, 2014; *Cecil et al.*, 2014].  
411 Namely, the diurnal cycle over land drives the overall global diurnal variability in lightning, with

412 the ocean flash rate essentially flat throughout the day and night. On average, lightning peaks  
413 in the local afternoon (3-4 pm Local Solar Time, LST), and reaches a minimum near 10 am LST  
414 (Fig. 9a). However, viewed in UTC time coordinates (Fig. 9b), lightning follows the classic  
415 Carnegie curve structure [Mach et al., 2011], peaking during 18-19 UTC.

416

### 417 *3.3 Use as a tool for GLM calibration and validation*

418 A high-priority effort at NASA MSFC has been to properly validate the GLM instruments  
419 on GOES-16 and GOES-17. This includes examining the GLM flash detection efficiency (DE), the  
420 flash false alarm rate, the lightning location/timing accuracy, maximum data rate capability, and  
421 long-term instrument degradation. Specific GLM instrument requirements have to be validated  
422 to confirm that GLM performance is acceptable for critical operations and decision making.  
423 GLM validation often makes use of several different ground-based lightning detection  
424 networks. These are high-quality data sources, but they are all land-based. A large part of the  
425 GLM FOV, especially GLM-17, is over the ocean where the quality of ground-truth data is highly  
426 variable. Fortunately, ISS LIS has provided vital data of uniform quality out over the oceans.

427 Another problem with comparing GLM to ground sources is that the comparison is not  
428 truly one-to-one. The GLM is an optical sensor, whereas all of the ground-based networks  
429 consist of RF sensors. The RF sensors look at fundamentally different physics and different parts  
430 of the lightning flash, making one-to-one comparisons difficult. Since ISS LIS is an optical sensor  
431 very similar to GLM, it is the only source of direct comparison for GLM. Indeed, because ISS LIS  
432 is a heritage sensor of GLM, with similar operation and data structure, it has provided

433 particularly easy/efficient inter-comparisons (i.e., both optical, both spaceborne, and both  
434 detect lightning over land/ocean).

435 GLM-16 has been observed to have a substantially depleted flash DE over the  
436 northwestern CONUS (e.g., Washington and surrounding states). A detailed plot of GLM-16  
437 flash DE for the period January 2018 to December 2019 is shown in Fig. 10. The GLM flashes  
438 were compared with observations from ISS LIS (Fig. 10 left), as well as data derived from two  
439 ground-based RF lightning detection networks - ENGLN (Fig. 10 middle) and GLD360 (Fig. 10  
440 right). All three comparison datasets agree on the basic structure of GLM-16's northwestern  
441 CONUS DE depletion. The fact that both optical spaceborne (ISS LIS) and RF ground-based  
442 (ENGLN and GLD360) measurements agree provides increased confidence that the DE depletion  
443 is the result of GLM instrument effects near the edges of its FOV.

444 ISS LIS continues to provide important one-to-one comparisons with GLM data, and will  
445 remain a key dataset for current and future GLM validation [e.g., *Zhang and Cummins, 2020*], as  
446 well as potentially other future geostationary lightning observations, such as from the  
447 forthcoming Meteosat Third Generation (MTG) Lightning Imager (LI). ISS LIS further provides a  
448 single observation system that will enable direct intercomparisons between GLM, LI, and other  
449 space-based observations.

450

### 451 *3.4 ISS LIS data products and user community*

452 Unlike its predecessor, ISS LIS has the ability to transmit and disseminate lightning data  
453 in near realtime. This ability is significant as it enables usage of ISS LIS in operational  
454 applications. The near-realtime capabilities are particularly beneficial in data-sparse regions,

455 such as over oceans, to contribute to storm warnings, nowcasts, oceanic aviation, and  
456 international Significant Meteorological advisories (SIGMETs). The near real-time ISS LIS data  
457 are provided to the US National Weather Service (NWS) and other interested users in  
458 partnership with both NASA's Land, Atmosphere Near real-time Capability for EOS (LANCE)  
459 project and the Short-term Prediction Research and Transition (SPoRT) center [*Jedlovec, 2013*].  
460 As ISS LIS detects total lightning (near globally) with high detection efficiency, it can therefore  
461 fill gaps in the depiction of lightning activity of interest to NWS forecasters over land and ocean  
462 areas. These data, as well as non-real-time analyses are being used by several applied and  
463 operational institutions to improve decision-making and to benefit humankind. These  
464 institutions include, for example, the NWS, the Aviation Weather Center (AWC), the National  
465 Hurricane Center (NHC), the Ocean Prediction Center (OPC), the World Weather Research  
466 Program (WWRP), and other government, business, and military organizations.

467         The GHRC DAAC coordinates with the LIS science team to process and archive the ISS LIS  
468 datasets. The ISS LIS mission currently produces four products: (1) Near-realtime (NRT) science  
469 lightning data [*Blakeslee, 2019a*], (2) NRT background cloud scene data [*Blakeslee, 2019b*], (3)  
470 Non-quality-controlled (NQC) version 1 science lightning data [*Blakeslee, 2019c*], and (4) NQC  
471 background cloud scene data [*Blakeslee, 2019d*].

472         The NRT data are available within two minutes of observation and are appropriate for  
473 applications requiring low-latency data (e.g., AWC and NHC). NRT data and browse images age  
474 off the server after ten days and are not a static archived data collection. Due to the nature of  
475 NRT data transmission, some data may be missing. Hence, the NQC data are produced daily and  
476 are more complete than the NRT data. Although the version 1 NQC data have not been

477 reviewed to assure data quality, they are more appropriate for science and applications with  
478 less stringent latency requirements. The version 1 NQC data have been validated, however, as  
479 described in Section 3.1, and are currently undergoing quality control that will be included in a  
480 future release.

481 The ISS LIS provides a variety of observations from the raw optical events that are  
482 combined into groups that are, in turn, combined into flashes as well as optical energy that can  
483 be used to observe lightning energetics. These base observations can be used to derive multiple  
484 products, as will be discussed below. Traditionally, the flash observation has been the most  
485 widely used, particularly in near real-time operations. This is a latitude/longitude point showing  
486 the centroid of the flash. This flash centroid is typically plotted as a density product (i.e.,  
487 number of flash centroids per 8 km<sup>2</sup>). Users can recreate this basic visualization capability via a  
488 python data recipe provided by GHRC DAAC [GHRC, 2020].

489 The ISS LIS dataset has had widespread use in the past 3 years, with over 6,100 users to  
490 date. Specifically, the GHRC DAAC has tallied downloads of the data based on the application  
491 science discipline. As with the OTD and TRMM LIS predecessors, there has always been an  
492 enthusiasm from the user community to apply lightning data in diverse ways, especially in  
493 weather and chemistry/climate studies. For the most recent full calendar year (2019), ISS LIS  
494 data made up two of the top five most downloaded datasets at GHRC DAAC. Two others,  
495 including the top dataset, were from the ISS LIS predecessor, TRMM LIS.

496 While not exhaustive, several uses of ISS LIS are described below, and demonstrate a  
497 variety of impacts by these observations. As mentioned previously, the near-realtime ISS LIS  
498 data are provided to the AWC. The AWC's area of responsibility covers vast oceanic regions.

499 The ISS LIS flash observations are vital to provide lightning observations in locations where  
500 ground networks are unavailable or have limited detection efficiency. Just a single flash  
501 observation provides confirmation of a convective system to the AWC, enabling aircraft to be  
502 rerouted safely around these systems. The near-realtime data have also been an integral  
503 component of the World Meteorological Organization's High Impact Weather Lake Systems  
504 (HIGHWAY) project [*Virts and Goodman, 2019*]. Centered on Lake Victoria in East Africa, the  
505 near-realtime ISS LIS data from NASA LANCE support local decision makers by helping better  
506 characterize storms as observed by the European Organization for the Exploitation of  
507 Meteorological Satellites (EUMETSAT) Meteosat Second Generation (MSG) satellite, and  
508 provide early warning to at-risk communities. This also serves as an operational demonstration  
509 to help prepare the community for MTG-LI.

510 Another collaborative project was with NASA DEVELOP and GHRC DAAC. Here, data  
511 from both TRMM and ISS LIS were used to develop a lightning risk assessment for Bangladesh  
512 and Nepal [*Evans et al., 2018*]. The LIS data provided the necessary lightning observations for  
513 the project. Instead of simply creating a lightning climatology, the DEVELOP team combined the  
514 lightning observations with socioeconomic information. The result (Fig. 11) gave the  
515 government authorities an easy-to-interpret view of where lightning was the greatest threat  
516 due to a combination of lightning activity, available shelter, and types of jobs. Such information  
517 can help government decision-makers direct funds to improve lightning safety in the most at-  
518 risk locations.

519 Lastly, the World Meteorological Organization has deemed lightning an Essential  
520 Climate Variable. Space-based observations play an integral role in providing global lightning

521 coverage. The ISS LIS observations extend the record of the earlier OTD and TRMM LIS  
522 instruments, and are included with those instruments in the Global Climate Observing System  
523 (GCOS). As part of this, ISS LIS observations will be used as part of a proposed 10x10 km<sup>2</sup>, global  
524 product that blends both space- and ground-based lightning observations into daily and  
525 monthly time scales [Aich et al., 2018].

526

#### 527 **4. Current and future cross-platform science**

528 Although ISS LIS observations have been used for assessments of current and future  
529 geostationary lightning mappers [Erdman et al., 2020; Hui et al., 2020], they also offer very  
530 complementary information for other types of atmospheric investigations.

531

##### 532 *4.1. Investigations into lightning discharge physics*

533 Comparisons of optical and RF emissions from lightning have provided a wealth of  
534 insights on processes involved in the lightning discharge [Suszcynsky et al., 2000; Thomas et al.,  
535 2000; Ushio et al., 2002; Noble et al., 2004; Zhang and Cummins, 2020]. Hence, the capability of  
536 ISS LIS to detect the optical fingerprint of lightning on a global scale with a relatively high  
537 detection efficiency makes for a unique dataset to compare with RF-based and other  
538 measurements of lightning and related atmospheric electrical phenomena.

539 Current and planned space-based missions to investigate lightning and upper  
540 atmospheric electrical phenomena include measurements across several parts of the  
541 electromagnetic spectrum that complement those obtained with ISS LIS. One of these is the  
542 Atmosphere-Space Interactions Monitor (ASIM), which is an instrument suite developed by the

543 European Space Agency and installed on the ISS in April 2018 [Neubert *et al.*, 2019]. The imager  
544 onboard ASIM has a 42x slower frame rate than LIS, but it has a 10x greater pixel resolution at  
545 nadir than the LIS camera [Chanrion *et al.*, 2019]. Furthermore, ASIM is capable of measuring  
546 light intensity across its FOV about 200x faster than LIS. This complementary nature of ASIM  
547 and LIS enables resolving the spatial and temporal components of lightning in more detail.

548 Both instruments detected a lightning flash on 7 February 2019, at 1941 UTC over  
549 Madagascar (Fig. 12). During its 150-ms duration, the flash illuminated three frames of the  
550 ASIM camera, while LIS detected nine groups. Figure 12 highlights one of these frames from the  
551 ASIM camera, along with the LIS events and temporal evolution of LIS groups and ASIM's 777.4-  
552 nm photometer. Each of the three LIS groups detected during this ASIM camera frame had a  
553 corresponding relative peak irradiance measured by the ASIM photometer. Although ASIM's  
554 photometer was able to detect these distinct flash subcomponents, LIS was used to locate  
555 where in ASIM's photometer FOV they occurred, which is especially important for separating  
556 multiple source regions within active thunderstorm complexes. One of the strokes illuminated  
557 36 pixels of the LIS camera for 2 ms, and the higher-resolution ASIM camera observations  
558 revealed the thinnest parts of that lightning channel to be roughly half a LIS pixel wide ( $\sim 2$  km).  
559 Hence, this comparison of the ASIM and LIS cameras provides insight into how the lightning  
560 channel geometry of this flash caused the intensity pattern detected by LIS.

561 Localized source extension below the LIS resolution and above the ASIM resolution can  
562 be intense enough to trigger a LIS event without the ability to infer the true spatial extent. Also,  
563 curved channels within one or more pixels and dark regions between emitting parts of a cloud  
564 may not be resolved by LIS. Instead, the intensity measured by LIS would be proportional to the

565 seemingly more active part of the cloud, obscuring whether the respective source was wider  
566 and less intense or small and bright. This is important because it has implications for  
567 characterizing the LIS sub-pixel variability of lightning and better understanding the physics of  
568 the lightning discharge.

569         Satellite missions such as ASIM and the upcoming Tool for Analysis of Radiation from  
570 lightning and Sprites (TARANIS) [Lefeuvre et al., 2008], which focus on investigating transient  
571 luminous events (TLEs) and terrestrial gamma ray flashes (TGFs), will be compared with  
572 observations from ISS LIS for calibration and validation of their optical instruments and used to  
573 better determine the spectral fingerprint of these upper atmospheric electrical phenomena.  
574 Additionally, LIS observations are being compared with ground-based electric field  
575 measurements from the Huntsville Alabama Marx Meter Array (HAMMA) [Bitzer et al., 2013]  
576 sensors deployed in Panama to investigate signatures of TGFs measured at the ground to their  
577 optical characteristics observed in space. The HAMMA sensors in Huntsville, Alabama, and  
578 Panama also are being compared with ISS LIS to observations to further investigate the extent  
579 of optical emissions by narrow bipolar events [Jacobson et al., 2013; Rison et al., 2016; Liu et  
580 al., 2018].

581

#### 582 *4.2. Precipitation and lightning in mid-latitude cyclones*

583         Since the ISS LIS operates during the era of the Global Precipitation Measurement  
584 (GPM) mission [Hou et al., 2014; Skofronick-Jackson et al., 2018], global observations of  
585 lightning and precipitation are being combined to expand upon related findings from TRMM in  
586 the tropics [Petersen and Rutledge, 2001; Liu et al., 2012] and gain new insights of mid- and

587 high-latitude storm systems. Coincident ISS LIS and GPM observations are being combined into  
588 a new lightning-enriched GPM-based Precipitation Feature (PF) dataset to facilitate these  
589 investigations. For example, this new dataset is being used to study the microphysical and  
590 dynamical response of the extratropical transition of tropical cyclones (TCs) [Gatlin *et al.*, 2019].  
591 ISS LIS is extremely important to this study since it enables inclusion of cyclones in the Pacific  
592 and Indian Oceans. The ISS LIS-enriched PF database dates to 2017, and the number of ISS and  
593 orbital GPM coincidences continue to increase with time, which should soon enable meaningful  
594 statistics on the convective characteristics of mid-latitude-transitioning TCs.

595

#### 596 *4.3. LNO<sub>x</sub> estimation for climate and air quality studies*

597 Lightning produces nitrogen oxides ( $\text{NO}_x = \text{NO} + \text{NO}_2$ ) that affects the concentration of  
598 greenhouse gases such as ozone [Huntrieser *et al.*, 1998]. Since climate is most sensitive to  
599 ozone in the upper troposphere, and since lightning is the most important source of  $\text{NO}_x$  in the  
600 upper troposphere at tropical and subtropical latitudes, lightning is a particularly useful  
601 parameter to monitor for climate assessments. Satellite-based optical lightning mappers have  
602 been used to make preliminary estimates of lightning  $\text{NO}_x$  (LNO<sub>x</sub>) and used to examine its  
603 interannual variability and begin monitoring the annual trend [Koshak, 2017]. Continuing these  
604 data records using ISS LIS observations is planned, and is particularly important for supporting  
605 the NCA program.

606 LNO<sub>x</sub> also impacts ozone estimates made by regional air quality models [e.g., Koshak *et*  
607 *al.*, 2014a]. Hence a better understanding of the contribution of LNO<sub>x</sub> to greenhouse gas  
608 pollution in the lower troposphere is needed. Also onboard the ISS is the Stratospheric Aerosol

609 and Gas Experiment (SAGE) III [Flittner et al., 2018], which provides observations of nitrogen  
610 dioxide (NO<sub>2</sub>) that will provide ideal comparisons with ISS LIS retrievals of LNO<sub>x</sub>. New  
611 geostationary instruments - Tropospheric Emissions: Monitoring of Pollution (TEMPO), Sentinel-  
612 4, and Geostationary Environment Monitoring Spectrometer (GEMS) - will provide unique NO<sub>2</sub>  
613 measurements [Zoogman et al., 2017; Courrèges-Lacoste et al., 2017; Kim et al., 2020] for  
614 comparison with ISS LIS. This combination of satellite-based chemistry measurements together  
615 with ISS LIS offer an unprecedented opportunity to fully probe LNO<sub>x</sub> production that is so vital  
616 to climate and air quality studies.

617

## 618 **5. Summary and conclusions**

619 ISS LIS has completed more than three years on orbit. During that time, it has met all of  
620 its major science objectives, including detection of lightning during day and night, at storm-  
621 scale (~4-km) spatial resolution, with millisecond timing and high flash detection efficiency (64%  
622 relative to a comparable optical sensor) without a land/ocean bias. ISS LIS also measures  
623 radiant energy, provides background images/intensity, and delivers near-realtime lightning  
624 data. In addition, it has produced a lightning climatology that is fundamentally consistent with  
625 previous lightning climatologies, while also enabling the extension of the climatologies into the  
626 current era as well as to higher latitudes ( $\pm 55^\circ$ ). Global flash rates (3-year average:  $\sim 44 \text{ s}^{-1}$ ) are  
627 within 5-10% of previous datasets [e.g., Cecil et al., 2014], and the spatial and diurnal  
628 distributions of global lightning are consistent with expectations. ISS LIS has demonstrated its  
629 value as a calibration/validation tool for current and future spaceborne lightning datasets. The  
630 near-realtime ISS LIS data have opened up applications within operational weather forecasting

631 and related applications, including public safety. Finally, ISS LIS is demonstrating utility as part  
632 (or potential part) of cross-platform studies examining a diverse array of topics, including  
633 lightning physics, thunderstorm processes, and atmospheric composition.

634 **Acknowledgements**

635 ISS LIS resulted from and with several key partnerships. The ISS Program Research  
636 Integration Office (PRIO) at NASA Johnson Space Center (JSC) provided funding for  
637 development, launch and integration of LIS. The ISS PRIO also funded the DoD Space Test  
638 Program (STP) to add LIS to the STP-H5 Payload. The NASA Science Mission Directorate Earth  
639 Science Division initially leveraged TRMM LIS science funding to cover ISS LIS science, and then  
640 transitioned this support in 2017 to the Earth from ISS program. NASA Marshall Space Flight  
641 Center (MSFC) partnered with University of Alabama Huntsville (UAH) to prepare the spare LIS  
642 for ISS, which included building the new Interface Unit (IFU), and MSFC partnered with NASA  
643 Goddard Space Flight Center to build key fiber optic harnesses for LIS. The LIS Science Team  
644 gratefully acknowledges the productive science and operations collaborations between MSFC,  
645 UAH, STP, Universities Space Research Association (USRA), and the ISS Payload Operations  
646 Integration Center. ISS-LIS and STP-5 were launched to the ISS from Kennedy Space Center  
647 (KSC) after integration onto a SpaceX rocket. ISS LIS data are available from the GHRC DAAC via  
648 the Digital Object Identifiers (DOIs) listed in the *Blakeslee* [2019a-d] references.

649 **References**

650 Aich, V., R. Holzworth, S. J. Goodman, Y. Kuleshov, C. Price, and E. Williams, 2018: Lightning: A  
651 new essential climate variable, *Eos*, 99, <https://doi.org/10.1029/2018EO104583>.

652  
653 Albrecht, R.I., S.J. Goodman, D.E. Buechler, R.J. Blakeslee, and H.J. Christian, 2016: Where Are  
654 the Lightning Hotspots on Earth?. *Bull. Amer. Meteor. Soc.*, 97, 2051–2068,  
655 <https://doi.org/10.1175/BAMS-D-14-00193.1>

656  
657 Bitzer, P. M., Christian, H. J., Stewart, M., Burchfield, J., Podgorny, S., Corredor, D., Hall, J.,  
658 Kuznetsov, E., and Franklin, V. ( 2013), Characterization and applications of VLF/LF source  
659 locations from lightning using the Huntsville Alabama Marx Meter Array, *J. Geophys. Res.*  
660 *Atmos.*, 118, 3120– 3138, doi:10.1002/jgrd.50271.

661  
662 Blakeslee, Richard J., 2019a. NRT Lightning Imaging Sensor (LIS) on International Space Station  
663 (ISS) Science Data. Dataset available online from the NASA Global Hydrology Resource Center  
664 DAAC, Huntsville, Alabama, U.S.A. <http://dx.doi.org/10.5067/LIS/ISSLIS/DATA106>.

665  
666 Blakeslee, Richard J., 2019b. NRT Lightning Imaging Sensor (LIS) on International Space Station  
667 (ISS) Backgrounds. Dataset available online from the NASA Global Hydrology Resource Center  
668 DAAC, Huntsville, Alabama, U.S.A. <http://dx.doi.org/10.5067/LIS/ISSLIS/DATA206>.

669

670 Blakeslee, Richard J., 2019c. Non-Quality Controlled Lightning Imaging Sensor (LIS) on  
671 International Space Station (ISS) Science Data. Dataset available online from the NASA Global  
672 Hydrology Resource Center DAAC, Huntsville, Alabama, U.S.A.  
673 <http://dx.doi.org/10.5067/LIS/ISSLIS/DATA107>.

674

675 Blakeslee, Richard J., 2019d. Non-Quality Controlled Lightning Imaging Sensor (LIS) on  
676 International Space Station (ISS) Backgrounds. Dataset available online from the NASA Global  
677 Hydrology Resource Center DAAC, Huntsville, Alabama, U.S.A.  
678 <http://dx.doi.org/10.5067/LIS/ISSLIS/DATA207>.

679

680 Blakeslee, R. J., Mach, D. M., Bateman, M. G., & Bailey, J. C. (2014). Seasonal variations in the  
681 lightning diurnal cycle and implications for the global electric circuit. *Atmospheric research*,  
682 135, 228-243.

683

684 Boccippio, D. J., W. J. Koshak, R. J. Blakeslee, 2002: Performance assessment of the Optical  
685 Transient Detector and Lightning Imaging Sensor. Part I: predicted diurnal variability, *J. Atmos.*  
686 *Oceanic Technol.*, 19, 1318-1332.

687

688 Buechler, D. E., Koshak, W. J., Christian, H. J., & Goodman, S. J. (2014). Assessing the  
689 performance of the Lightning Imaging Sensor (LIS) using deep convective clouds. *Atmospheric*  
690 *research*, 135, 397-403.

691

692 Cecil, D. J., Buechler, D. E., & Blakeslee, R. J. (2014). Gridded lightning climatology from TRMM-  
693 LIS and OTD: Dataset description. *Atmospheric Research*, 135, 404-414.

694

695 Chanrion, O., Neubert, T., Lundgaard Rasmussen, I. et al. The Modular Multispectral Imaging  
696 Array (MMIA) of the ASIM Payload on the International Space Station. *Space Sci Rev* 215, 28  
697 (2019). <https://doi.org/10.1007/s11214-019-0593-y>

698

699 Christian, H. J., Blakeslee, R. J., and Goodman, S. J. (1989), The detection of lightning from  
700 geostationary orbit, *J. Geophys. Res.*, 94( D11), 13329– 13337, doi:10.1029/JD094iD11p13329.

701

702 Christian, H. J., et al., Global frequency and distribution of lightning as observed from space by  
703 the Optical Transient Detector, *J. Geophys. Res.*, 108( D1), 4005, doi:10.1029/2002JD002347,  
704 2003.

705

706 Christian, H. J., R. L. Frost, P. H. Gillaspy, S. J. Goodman, O. H. Vaughan, M. Brook, B. Vonnegut,  
707 and R. E. Orville (1983), Observations of optical lightning emissions from above thunderstorms  
708 using U-2 aircraft, *Bull. Am. Meteorol. Soc.*, 64, 120–123. doi: 0.1175/1520-  
709 0477(1983)064<0120:OOOLEF>2.0.CO;2.

710

711 Courrèges-Lacoste, G. B. M. Sallusti, G. Balsa, G. Bagnasco, Ben Veihelmann, S. Riedl, D. J.  
712 Smith, R. Maurer, 2017: The Copernicus Sentinel 4 mission: a geostationary imaging UVN

713 spectrometer for air quality monitoring, Proc. SPIE 10423, Sensors, Systems, and Next-  
714 Generation Satellites XXI, 1042307. doi: 10.1117/12.2282158

715

716 Darden, C.B., D.J. Nadler, B.C. Carcione, G.T. Stano, and D.E. Buechler, 2009: Utilizing total  
717 lightning information to diagnose convective trends. Bull. Amer. Meteor. Soc., 91, 167-175. doi:  
718 <http://dx.doi.org/10.1175/2009BAMS2808.1>

719

720 Earthdata, cited 2020. NASA Earthdata Search. [Available online at  
721 [https://search.earthdata.nasa.gov/.](https://search.earthdata.nasa.gov/)]

722

723 Erdmann, F., Defer, E., Caumont, O., Blakeslee, R. J., Pédeboy, S., and Coquillat, S.: Concurrent  
724 satellite and ground-based lightning observations from the Optical Lightning Imaging Sensor  
725 (ISS-LIS), the low-frequency network Meteorage and the SAETTA Lightning Mapping Array  
726 (LMA) in the northwestern Mediterranean region, Atmos. Meas. Tech., 13, 853–875, doi:  
727 10.5194/amt-13-853-2020, 2020.

728

729 Evans, C., S. Shrestha, E. Raphael, J. Luvall, R. Griffin, and P. Gatlin, 2018: Hindu-Kush Himalayan  
730 Disasters. Integrating NASA Earth observations to monitor intense thunderstorms and assess  
731 lightning exposure and risk in the Hindu-Kush Himalayan region. NASA DEVELOP Technical  
732 Report., 19 pp.

733

734 Flittner, D., Thomason, L., Hill, C., Roell, M., Pitts, M., Damadeo, R., ... & Stanley, R. (2018, April).  
735 Stratospheric Aerosol and Gas Experiment III installed on the International Space Station (SAGE  
736 III/ISS): Overview. In EGU General Assembly Conference Abstracts (Vol. 20, p. 5483).  
737

738 Gatlin, P., L. Huescher, C. Liu, W. Petersen, D. J. Cecil, 2019: The evolution and extratropical  
739 transition of tropical cyclones from a GPM, ISS LIS and GLM perspective, AGU 2019 Fall  
740 Meeting, December 9-13, 2019, San Francisco, CA, American Geophysical Union, H13P-1976.  
741

742 Global Hydrology Resource Center, cited 2020. ISS LIS Lightning Flash Location Quickview using  
743 Python 3.0 and GIS. [Available online at [https://ghrc.nsstc.nasa.gov/home/data-recipes/iss-lis-](https://ghrc.nsstc.nasa.gov/home/data-recipes/iss-lis-lightning-flash-location-quickview-using-python-30-and-gis)  
744 [lightning-flash-location-quickview-using-python-30-and-gis](https://ghrc.nsstc.nasa.gov/home/data-recipes/iss-lis-lightning-flash-location-quickview-using-python-30-and-gis)].  
745

746 Goodman, S. J., R. J. Blakeslee, W. J. Koshak, D. Mach, J. Bailey, D. Buechler, L. Carey, C. Schultz,  
747 M. Bateman, E. McCaul, G. Stano, The GOES-R Geostationary Lightning Mapper (GLM),  
748 Atmospheric Research, Volumes 125–126, 2013, Pages 34-49, ISSN 0169-8095,  
749 <https://doi.org/10.1016/j.atmosres.2013.01.006>.  
750

751 Hou, A.Y., Kakar, R.K., Neeck, S., Azarbarzin, A.A., Kummerow, C.D., Kojima, M., Oki, R.,  
752 Nakamura, K. and Iguchi, T. (2014) The global precipitation measurement mission. Bulletin of  
753 the American Meteorological Society, 95, 701–722. doi:10.1175/BAMS-D-13-00164.1.  
754

755 Hui, W., F. Huang and R. Liu (2020) Characteristics of lightning signals over the Tibetan Plateau  
756 and the capability of FY-4A LMI lightning detection in the Plateau, International Journal of  
757 Remote Sensing, 41, 4605-4625, doi: 10.1080/01431161.2020.1723176.

758  
759 Huntrieser, H., Schlager, H., Feigl, C., and Höller, H. ( 1998), Transport and production of NO X in  
760 electrified thunderstorms: Survey of previous studies and new observations at midlatitudes, J.  
761 Geophys. Res., 103( D21), 28247– 28264, doi:10.1029/98JD02353.

762  
763 HyDRO, cited 2020. NASA Hydrology Data Search Tool. [Available online at  
764 <https://ghrc.nsstc.nasa.gov/hydro.>]

765  
766 ISS LIS, cited 2020. ISS LIS Datasets. [Available online at  
767 [https://ghrc.nsstc.nasa.gov/lightning/data/data\\_lis\\_iss.html.](https://ghrc.nsstc.nasa.gov/lightning/data/data_lis_iss.html.)]

768  
769 Jacobson, A. R., Light, T. E. L., Hamlin, T., and Nemzek, R.: Joint radio and optical observations of  
770 the most radio-powerful intracloud lightning discharges, Ann. Geophys., 31, 563–580,  
771 <https://doi.org/10.5194/angeo-31-563-2013>, 2013.

772  
773 Jedlovec, G., 2013: Transitioning research satellite data to the operational weather community:  
774 The SPoRT paradigm. IEEE Geoscience and Remote Sensing Magazine, 1, no. 1, 62–66,  
775 <https://doi.org/10.1109/MGRS.2013.2244704>.

776

777 Kim, J. and Coauthors, 2020: New era of air quality monitoring from space: Geostationary  
778 Environment Monitoring Spectrometer (GEMS). Bull. Amer. Meteor. Soc., E1-E22. doi:  
779 10.1175/BAMS-D-18-0013.1.

780  
781 Koshak, W. (2017). Lightning-Related Indicators for National Climate Assessment (NCA) Studies.  
782 Fall Meeting 2017, American Geophysical Union, New Orleans, LA.

783  
784 Koshak, W. J., K. L. Cummins, D. E. Buechler, B. Vant-Hull, R. J. Blakeslee, E. R. Williams, H. S.  
785 Peterson, 2015: Variability of CONUS Lightning in 2003-12 and Associated Impacts, J. Appl.  
786 Meteorol. Climatology, 54, No. 1, 15-41.

787  
788 Koshak, W. J., B. Vant-Hull, E. W. McCaul, and H. S. Peterson, Variation of a lightning NOx  
789 indicator for national climate assessment, XV International Conference on Atmospheric  
790 Electricity, Norman, Oklahoma, June 15-20, 2014a.

791  
792 Koshak, W. J., H. S. Peterson, A. P. Biazar, M. N. Khan, and L. Wang, 2014b: The NASA Lightning  
793 Nitrogen Oxides Model (LNOM): Application to air quality modeling, Atmos. Res., 135-136, 363-  
794 369, doi:10.1016/j.atmosres.2012.12.015.

795  
796 Koshak, W. J., M. F. Stewart, H. J. Christian, J. W. Bergstrom, J. M. Hall, and R. J. Solakiewicz,  
797 2000: Laboratory Calibration of the Optical Transient Detector and the Lightning Imaging  
798 Sensor, J. Atmos. Oceanic Technol., 17, 905-915.

799

800 Kummerow, C., W. Barnes, T. Kozu, J. Shiue, and J. Simpson, 1998: The Tropical Rainfall  
801 Measuring Mission (TRMM) Sensor Package. *J. Atmos. Oceanic Technol.*, 15, 809–817,  
802 [https://doi.org/10.1175/1520-0426\(1998\)015<0809:TTRMMT>2.0.CO;2](https://doi.org/10.1175/1520-0426(1998)015<0809:TTRMMT>2.0.CO;2)

803

804 Lefeuvre, F., Blanc, E., Pinçon, J. et al. TARANIS—A Satellite Project Dedicated to the Physics of  
805 TLEs and TGFs. *Space Sci Rev* 137, 301–315 (2008). doi: 10.1007/s11214-008-9414-4.

806

807 Liu, C., Cecil, D. J., Zipser, E. J., Kronfeld, K., and Robertson, R. ( 2012), Relationships between  
808 lightning flash rates and radar reflectivity vertical structures in thunderstorms over the tropics  
809 and subtropics, *J. Geophys. Res.*, 117, D06212, doi:10.1029/2011JD017123.

810

811 Liu, F., Zhu, B., Lu, G., Qin, Z., Lei, J., Peng, K.-M., et al. ( 2018). Observations of blue discharges  
812 associated with negative narrow bipolar events in active deep convection. *Geophysical  
813 Research Letters*, 45, 2842– 2851. doi: 10.1002/2017GL076207.

814

815 Mach, D. M., Blakeslee, R. J., and Bateman, M. G. ( 2011), Global electric circuit implications of  
816 combined aircraft storm electric current measurements and satellite-based diurnal lightning  
817 statistics, *J. Geophys. Res.*, 116, D05201, doi:10.1029/2010JD014462.

818

819 Medici, G., K. L. Cummins, D. J. Cecil, W. J. Koshak, and S. D. Rudlosky, 2017: The intracloud  
820 lightning fraction in the contiguous United States. *Mon. Wea. Rev.*, 145, 4481–4499, doi:  
821 10.1175/MWR-D-16-0426.1.

822

823 Neubert, T., Østgaard, N., Reglero, V. et al. The ASIM Mission on the International Space  
824 Station. *Space Sci Rev* 215, 26 (2019). doi: 10.1007/s11214-019-0592-z.

825

826 Noble, C. M. M., Beasley, W. H., Postawko, S. E., and Light, T. E. L. ( 2004), Coincident  
827 observations of lightning by the FORTE photodiode detector, the New Mexico Tech Lightning  
828 Mapping Array and the NLDN during STEPS, *Geophys. Res. Lett.*, 31, doi:  
829 10.1029/2003GL018989.

830

831 Petersen, W.A. and S.A. Rutledge, 2001: Regional Variability in Tropical Convection:  
832 Observations from TRMM. *J. Climate*, 14, 3566–3586, [https://doi.org/10.1175/1520-](https://doi.org/10.1175/1520-0442(2001)014<3566:RVITCO>2.0.CO;2)  
833 [0442\(2001\)014<3566:RVITCO>2.0.CO;2](https://doi.org/10.1175/1520-0442(2001)014<3566:RVITCO>2.0.CO;2)

834

835 Rison, W., Krehbiel, P., Stock, M. et al. Observations of narrow bipolar events reveal how  
836 lightning is initiated in thunderstorms. *Nat Commun* 7, 10721 (2016). doi:  
837 10.1038/ncomms10721.

838

839 Rudlosky, S. D., Goodman, S. J., Virts, K. S., & Bruning, E. C. ( 2019). Initial geostationary  
840 lightning mapper observations. *Geophysical Research Letters*, 46, 1097–1104.  
841 <https://doi.org/10.1029/2018GL081052>

842

843 Saunders, C., 2008: Charge separation mechanisms in clouds, *Space Sci. Rev.*, 137, 335-353, doi  
844 10.1007/s11214-008-9345-0.

845

846 Skofronick-Jackson, G, Kirschbaum, D, Petersen, W, et al. The Global Precipitation  
847 Measurement (GPM) mission's scientific achievements and societal contributions: reviewing  
848 four years of advanced rain and snow observations. *Q J R Meteorol Soc* 2018; 144, 27–48. doi:  
849 10.1002/qj.3313

850

851 Suszcynsky, D. M., Kirkland, M. W., Jacobson, A. R., Franz, R. C., Knox, S. O., Guillen, J. L. L., and  
852 Green, J. L. (2000), FORTE observations of simultaneous VHF and optical emissions from  
853 lightning: Basic phenomenology, *J. Geophys. Res.*, 105, 2191–2201, doi:10.1029/1999JD900993.

854

855 Thomas, R. J., Krehbiel, P. R., Rison, W., Hamlin, T., Boccippio, D. J., Goodman, S. J., and  
856 Christian, H. J.: Comparison of ground-based 3-dimensional lightning mapping observations  
857 with satellite-based LIS observations in Oklahoma, *Geophys. Res. Lett.*, 27, 1703–1706, doi:  
858 10.1029/1999GL010845, 2000.

859

860 Ushio, T., S. Heckman, K. Driscoll, D. Boccippio, H. Christian, and Z. I. Kawasaki, 2002: Cross-  
861 sensor comparison of the Lightning Imaging Sensor (LIS), *International Journal of Remote*  
862 *Sensing*, 23, 2703-2712, doi: 10.1080/01431160110107789.

863  
864 Virts, K.S. and S.J. Goodman, 0: Prolific Lightning and Thunderstorm Initiation over the Lake  
865 Victoria Basin in East Africa. *Mon. Wea. Rev.*, 0, <https://doi.org/10.1175/MWR-D-19-0260.1>

866  
867 Virts, K.S., J.M. Wallace, M.L. Hutchins, and R.H. Holzworth, 2013: Highlights of a New Ground-  
868 Based, Hourly Global Lightning Climatology. *Bull. Amer. Meteor. Soc.*, 94, 1381–1391,  
869 <https://doi.org/10.1175/BAMS-D-12-00082.1>

870  
871 Yoshida, S., T. Adachi, K. Kusunoki, S. Hayashi, T. Wu, T. Ushio, and E. Yoshikawa, 2017:  
872 Relationship between thunderstorm electrification and storm kinetics revealed by phased array  
873 weather radar, *J. Geophys. Res. Atmos.*, 122, 3821–3836, doi:10.1002/ 2016JD025947.

874  
875 Zhang, D., & Cummins, K. L. (2020). Time evolution of satellite-based optical properties in  
876 lightning flashes, and its impact on GLM flash detection. *Journal of Geophysical Research:*  
877 *Atmospheres*, 125, e2019JD032024. doi: 10.1029/2019JD032024

878  
879 Zoogman, P. and Coauthors, 2017: Tropospheric Emissions: Monitoring of Pollution (TEMPO), *J.*  
880 *Quant. Spectrosc. Ra.*, 186, 17-39. doi: 10.1016/j.jqsrt.2016.05.008.

881

882 **Tables**

883 **Table 1.** ISS LIS global flash rate ( $s^{-1}$ ) versus the space-based TRMM LIS/OTD climatology [*Cecil*  
 884 *et al.*, 2014].

885

<b>Region</b>	<b>Annual</b>	<b>MAM</b>	<b>JJA</b>	<b>SON</b>	<b>DJF</b>
TRMM LIS/OTD World	45.7	44.1	55.7	47.2	35.9
ISS LIS < 55°	43.8	45.1	53.5	45.6	30.8
TRMM LIS/OTD < 38°	40.7	40.9	42.5	44.6	34.9
ISS LIS < 38°	39.5	42.8	41.0	43.8	30.3

886

887 **Figure Captions**

888

889 **Figure 1.** Visualization of the ISS LIS instrument, its location on the ISS, as well as its data  
890 collection, processing, and distribution.

891

892 **Figure 2.** Basic workflow showing the data processing of initial observations at the ISS through  
893 ground processing by GHRC and the LIS science team, to publication for end users.

894

895 **Figure 3.** The close comparison between the original TRMM LIS calibration (OC; labeled TRMM)  
896 and the retest calibration (RC) of ISS LIS (labeled ISS). Left: Static Response Test. Right: Transient  
897 Response Test.

898

899 **Fig. 4.** Left: ISS LIS temporal offset relative to ENGLN, GLD360, GLM-16, and GLM-17. Right: ISS  
900 LIS spatial geolocation offset relative to these comparison datasets.

901

902 **Figure 5.** Top: Time series of peak temporal offset between ISS LIS and three difference  
903 reference datasets (ENGLN, GLD360, and GLM-16). Middle: Time series of peak spatial offset  
904 between ISS LIS and these reference datasets. Bottom: Time series of ISS LIS DE and FAR  
905 relative to the reference datasets.

906

907 **Figure 6.** a) Three-year (March 2017 through February 2020) climatology of global lightning  
908 from ISS LIS. b) Post-boost climatology of lightning from TRMM LIS (September 2001 through  
909 December 2014).

910

911 **Figure 7.** Monthly time series of global lightning flash rate (between  $\pm 38^\circ$  latitude) from TRMM  
912 LIS and ISS LIS.

913

914 **Figure 8.** ISS LIS lightning climatology, broken out seasonally. a) March-May. b) June-August. c)  
915 September-November. d) December-February.

916

917 **Figure 9.** ISS LIS diurnal variability of global lightning flash rate, including land/ocean  
918 breakdown. a) Adjusted to local solar time. b) UTC time.

919

920 **Figure 10.** GLM-16 flash DE with respect to ISS LIS (left), ENGLN (middle), and GLM360 (right).

921

922 **Figure 11.** Lightning risk analysis for Nepal and Bangladesh, based on a combination of LIS flash  
923 rates and socioeconomic factors.

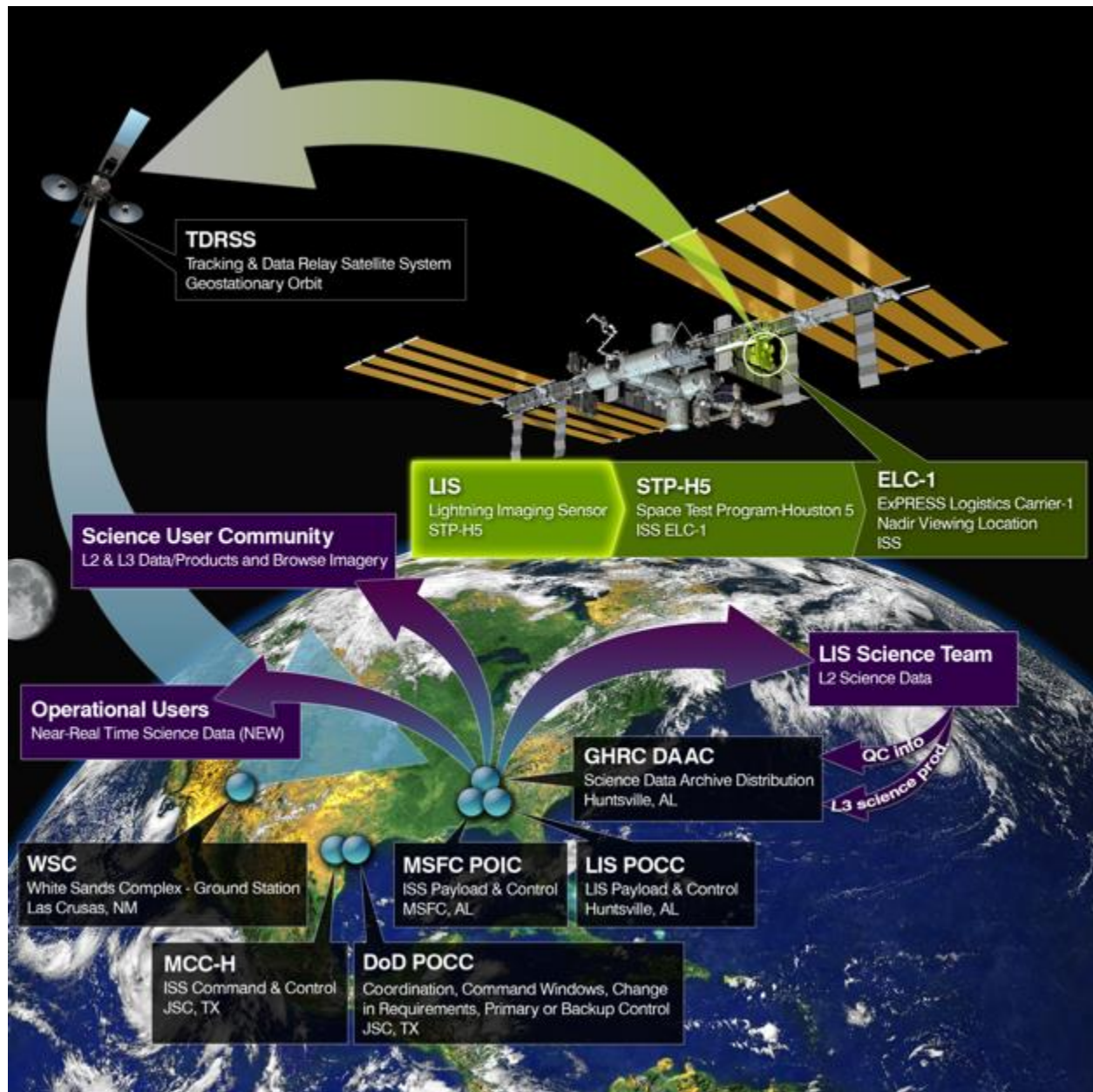
924

925 **Figure 12.** Comparison of ASIM and ISS LIS observations of a lightning flash over Madagascar.

926 (top) an image of the lightning flash captured by the ASIM camera with ISS LIS events from the  
927 group closest in time to the frame (i.e., black line in bottom panel) plotted as green symbols

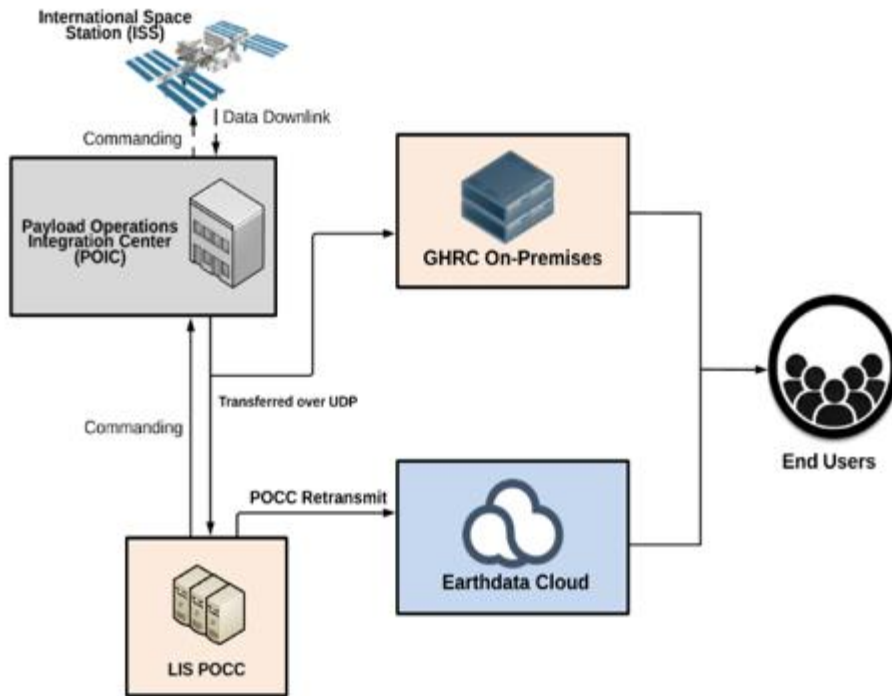
928 whose size correspond to the radiance measured by the LIS camera and scaled ( $10^{-4}$ ) to match

929 the same units of ASIM radiance, which are given in logarithmic scale to enhance the  
930 illuminated pixels. (bottom) time-series of ASIM 777.4 nm photometer (red) and LIS groups  
931 (green) with the shaded region corresponding to the duration of the ASIM camera frame.



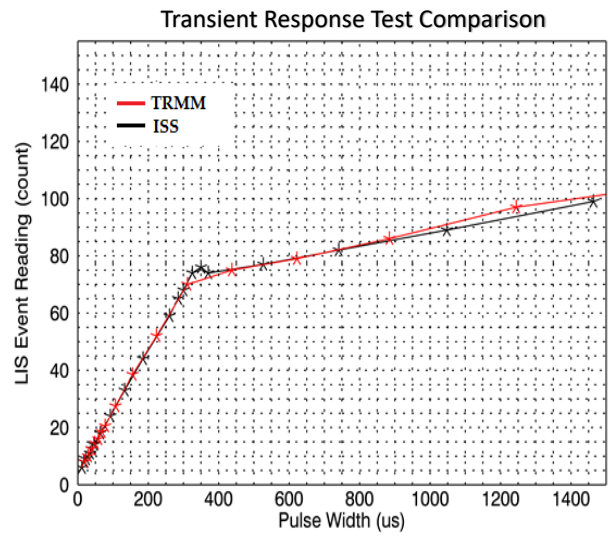
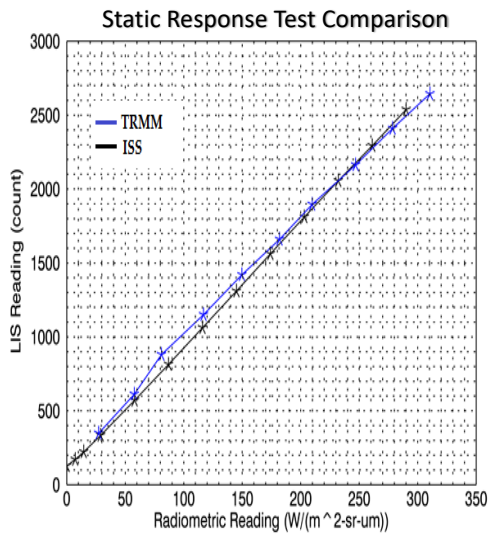
933

934 **Figure 1.** Visualization of the ISS LIS instrument, its location on the ISS, as well as its data  
 935 collection, processing, and distribution.



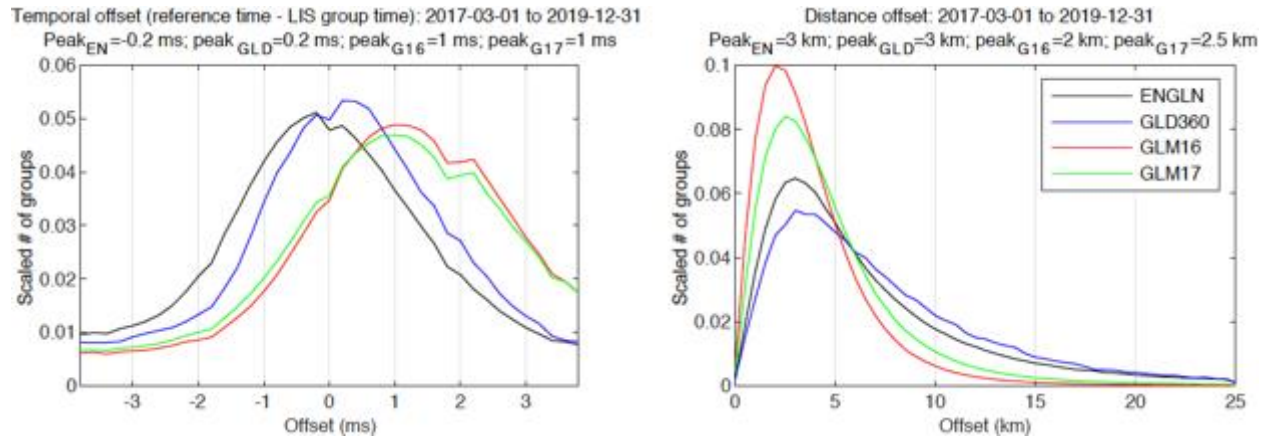
936

937 **Figure 2.** Basic workflow showing the data processing of initial observations at the ISS through  
 938 ground processing by GHRC and the LIS science team, to publication for end users.



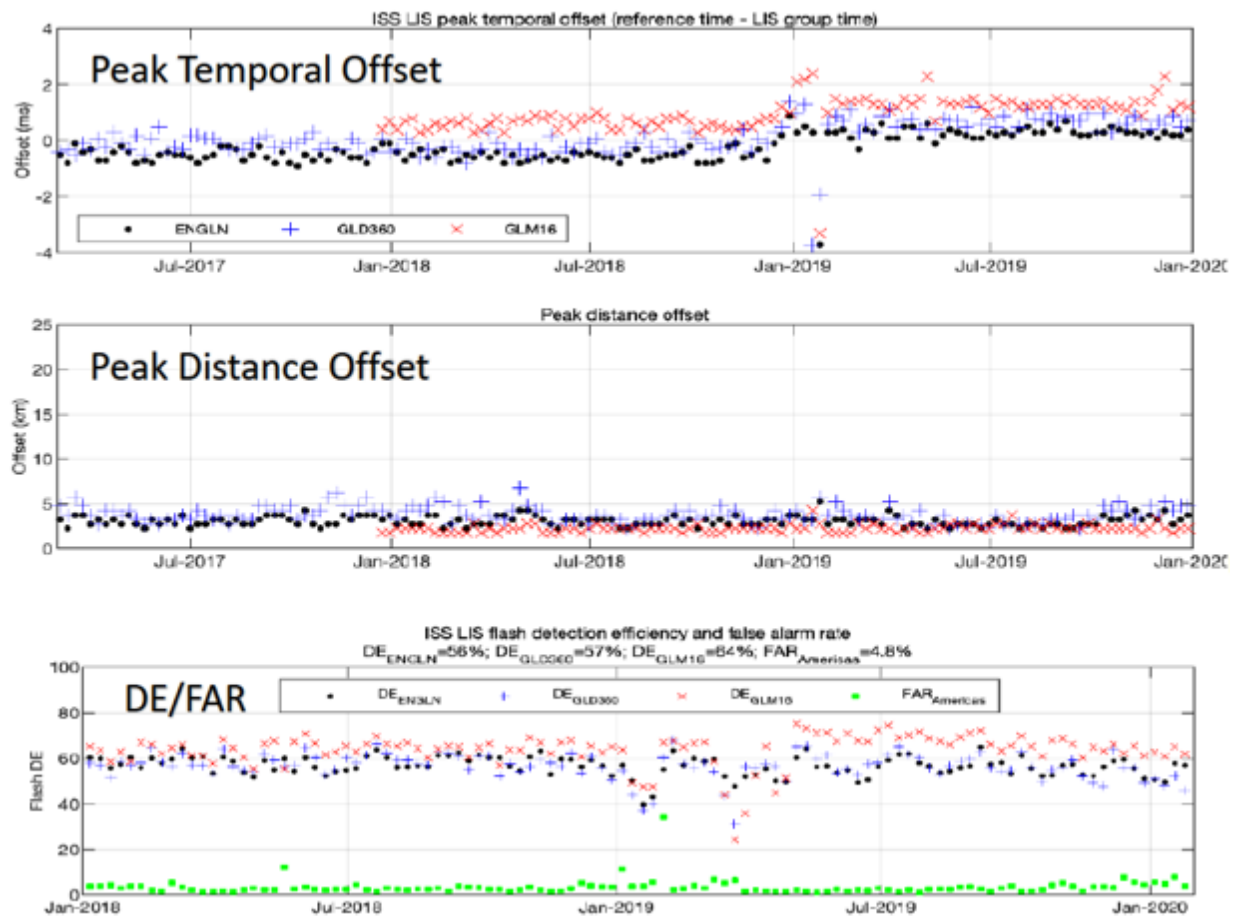
939

940 **Figure 3.** The close comparison between the original TRMM LIS calibration (OC; labeled TRMM)  
 941 and the retest calibration (RC) of ISS LIS (labeled ISS). Left: Static Response Test. Right: Transient  
 942 Response Test.



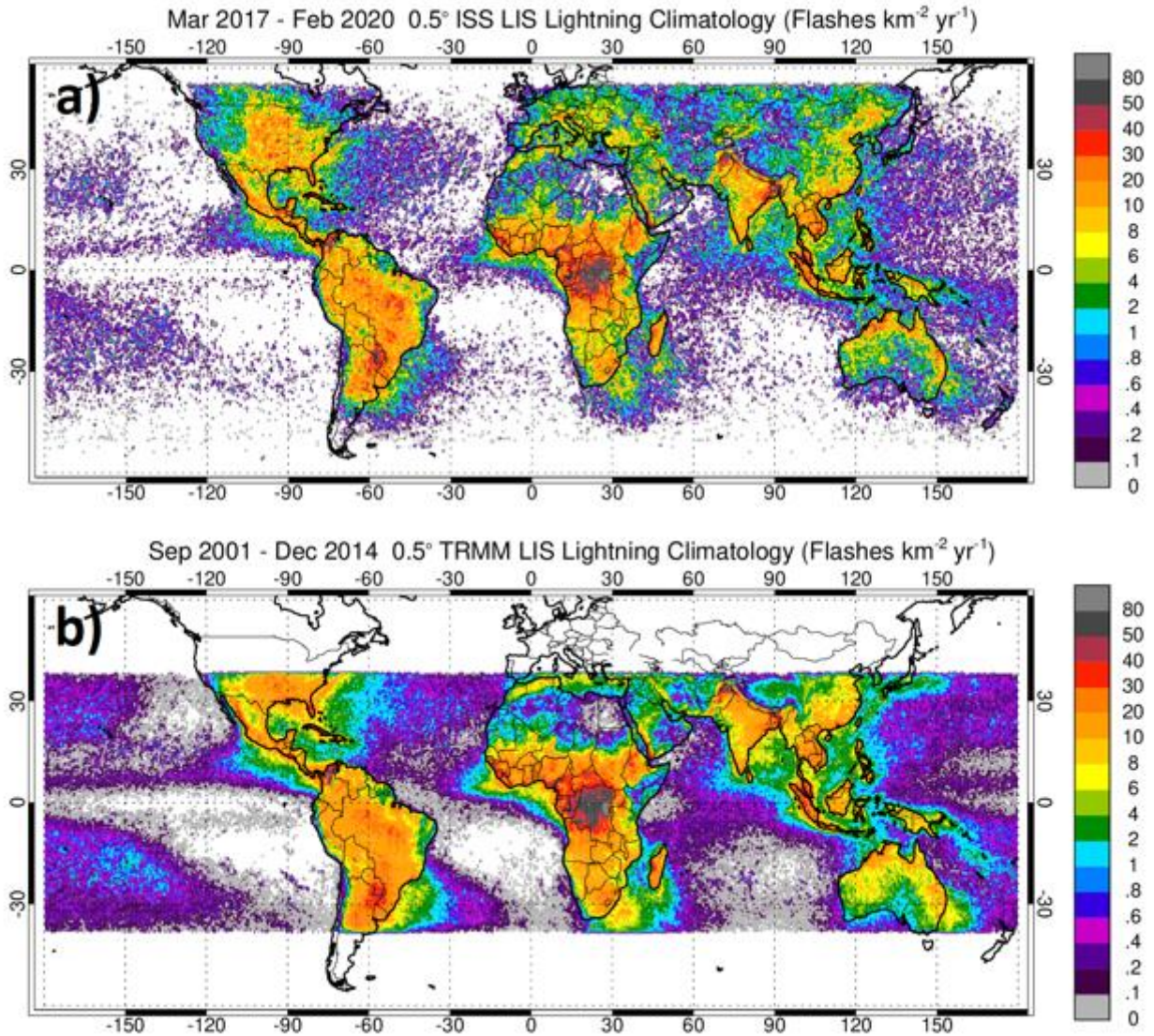
943

944 **Fig. 4.** Left: ISS LIS temporal offset relative to ENGLN, GLD360, GLM-16, and GLM-17. Right: ISS  
 945 LIS spatial geolocation offset relative to these comparison datasets.



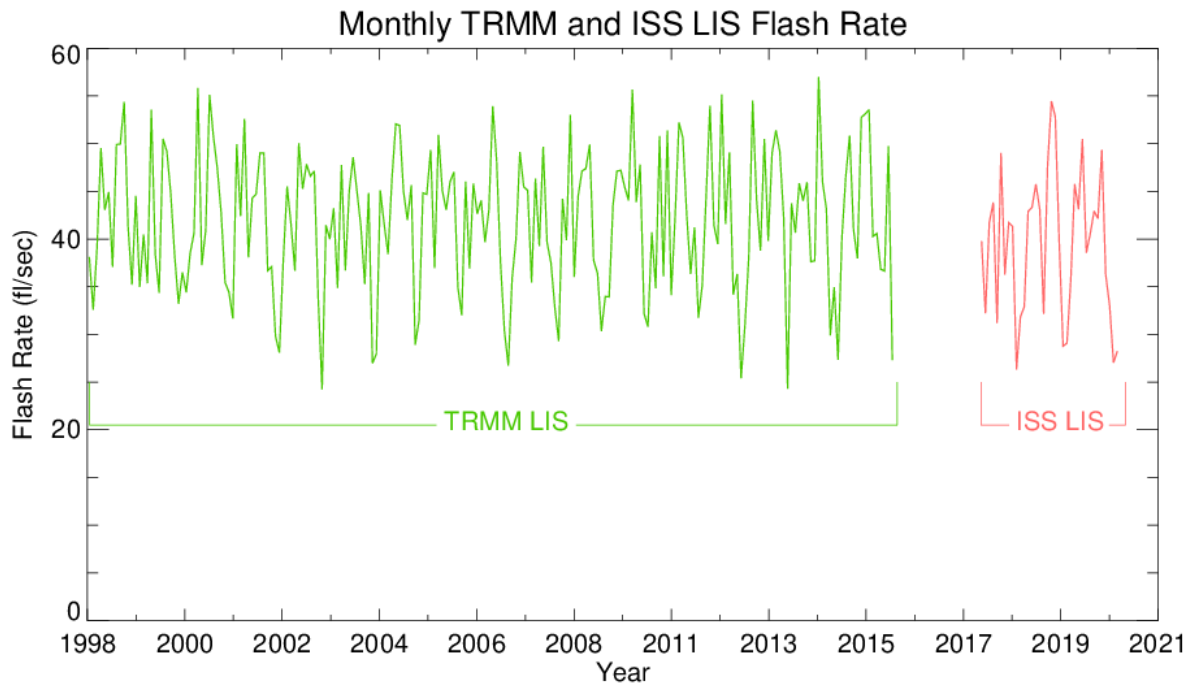
946

947 **Figure 5.** Top: Time series of peak temporal offset between ISS LIS and three difference  
 948 reference datasets (ENGLN, GLD360, and GLM-16). Middle: Time series of peak spatial offset  
 949 between ISS LIS and these reference datasets. Bottom: Time series of ISS LIS DE and FAR  
 950 relative to the reference datasets.



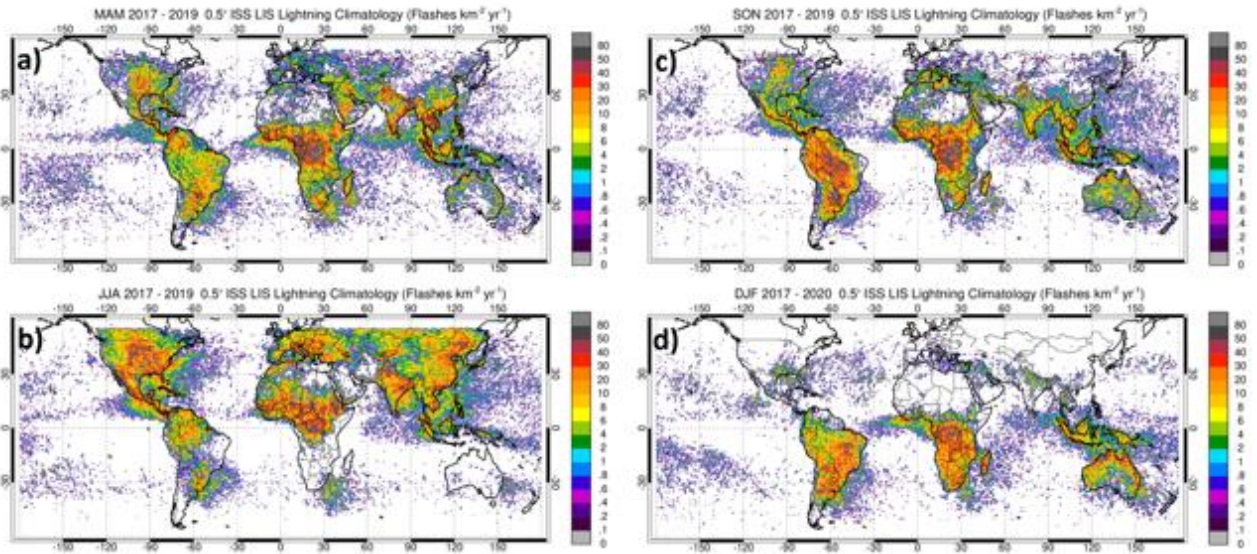
951

952 **Figure 6.** a) Three-year (March 2017 through February 2020) climatology of global lightning  
 953 from ISS LIS. b) Post-boost climatology of lightning from TRMM LIS (September 2001 through  
 954 December 2014).



955

956 **Figure 7.** Monthly time series of global lightning flash rate (between  $\pm 38^\circ$  latitude) from TRMM  
 957 LIS and ISS LIS.

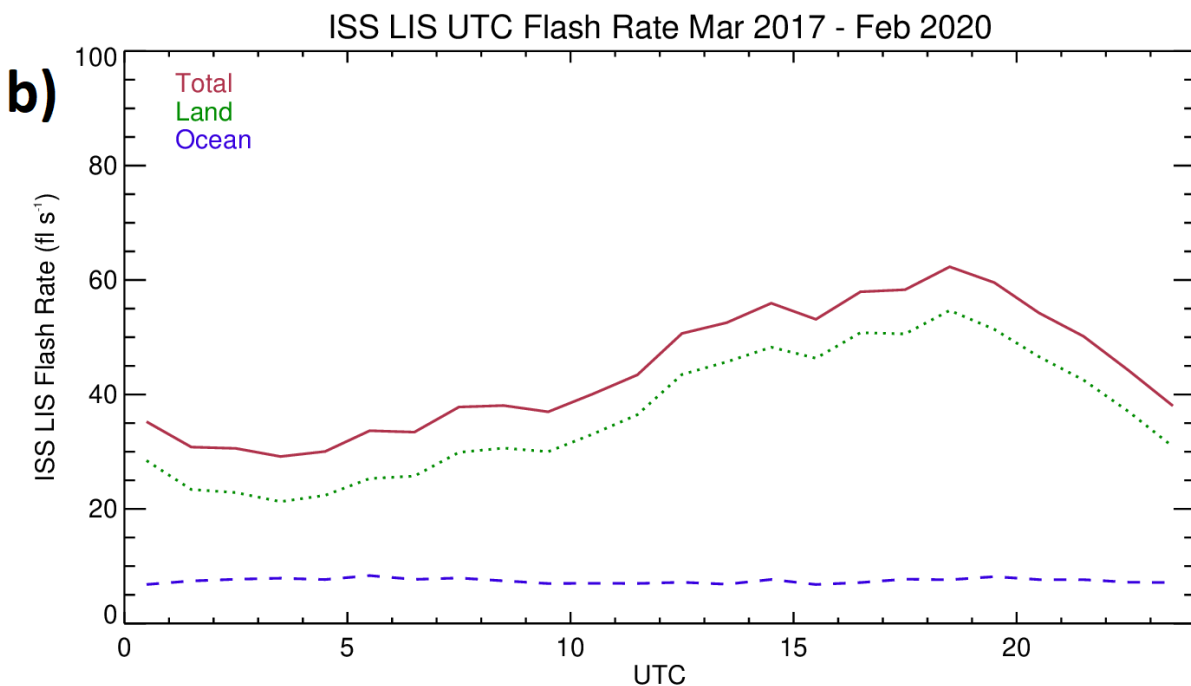
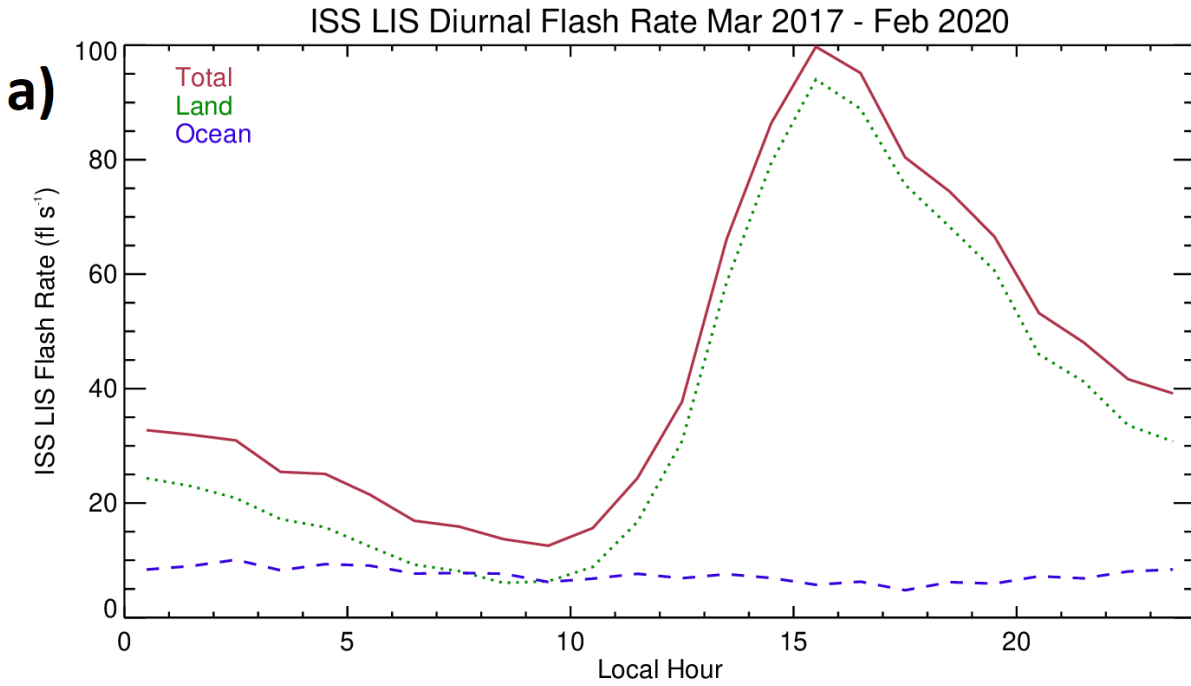


958

959 **Figure 8.** ISS LIS lightning climatology, broken out seasonally. a) March-May. b) June-August. c)  
 960 September-November. d) December-February.

961

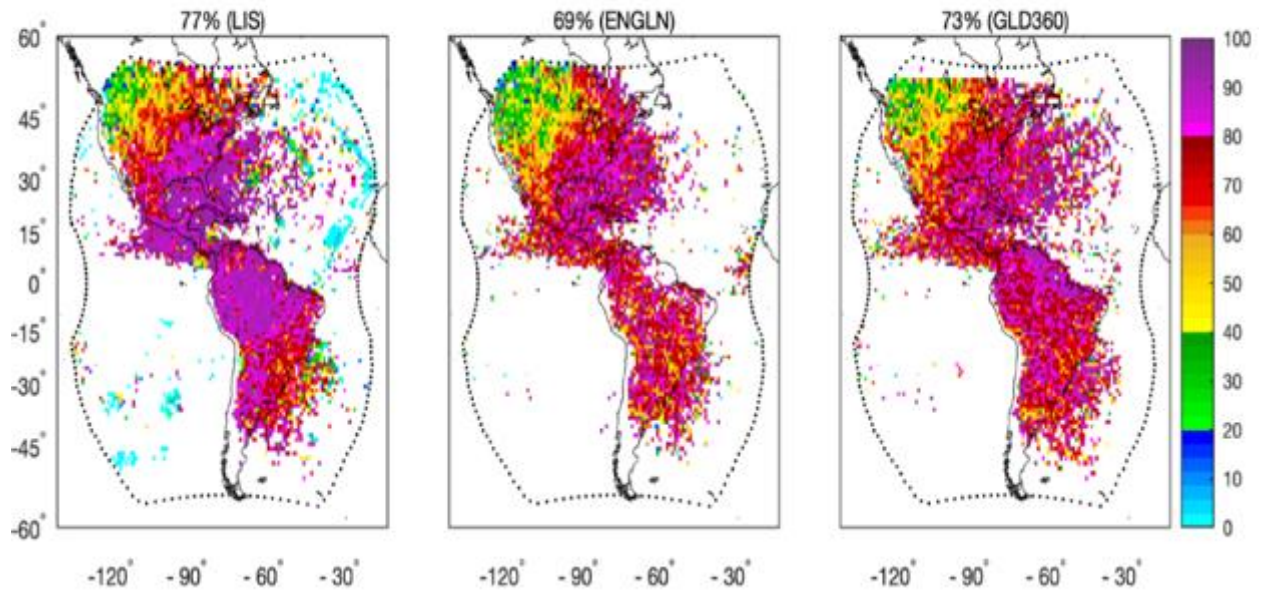
962 *(Reviewers: Please see original figure to obtain full resolution)*



963

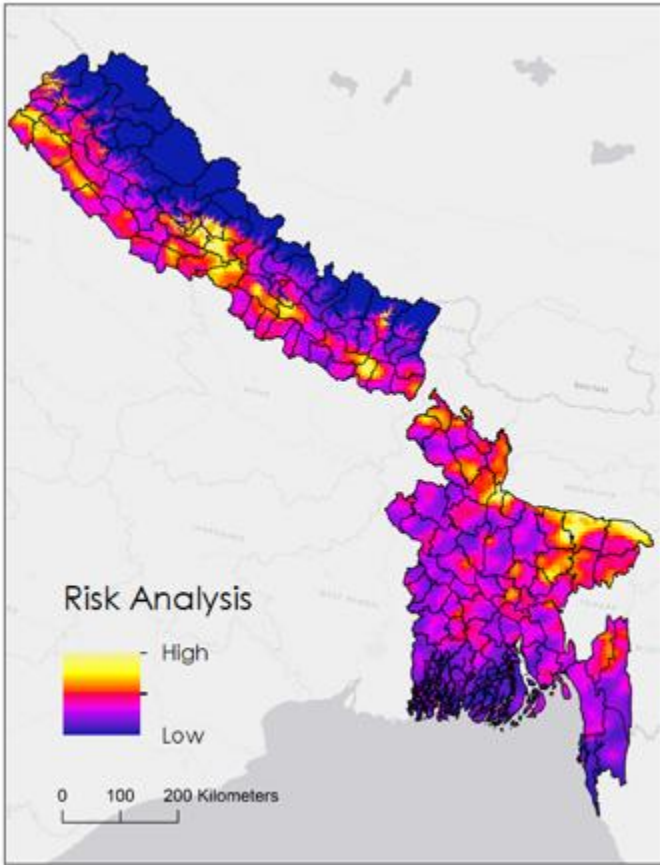
964 **Figure 9.** ISS LIS diurnal variability of global lightning flash rate, including land/ocean  
 965 breakdown. a) Adjusted to local solar time. b) UTC time.

GLM-16 flash DE with respect to reference data  
Matching window = 200 ms, 50 km; 2018-01-01 to 2019-12-31



966

967 **Figure 10.** GLM-16 flash DE with respect to ISS LIS (left), ENGLN (middle), and GLM360 (right).



968

969 **Figure 11.** Lightning risk analysis for Nepal and Bangladesh, based on a combination of LIS flash  
970 rates and socioeconomic factors.

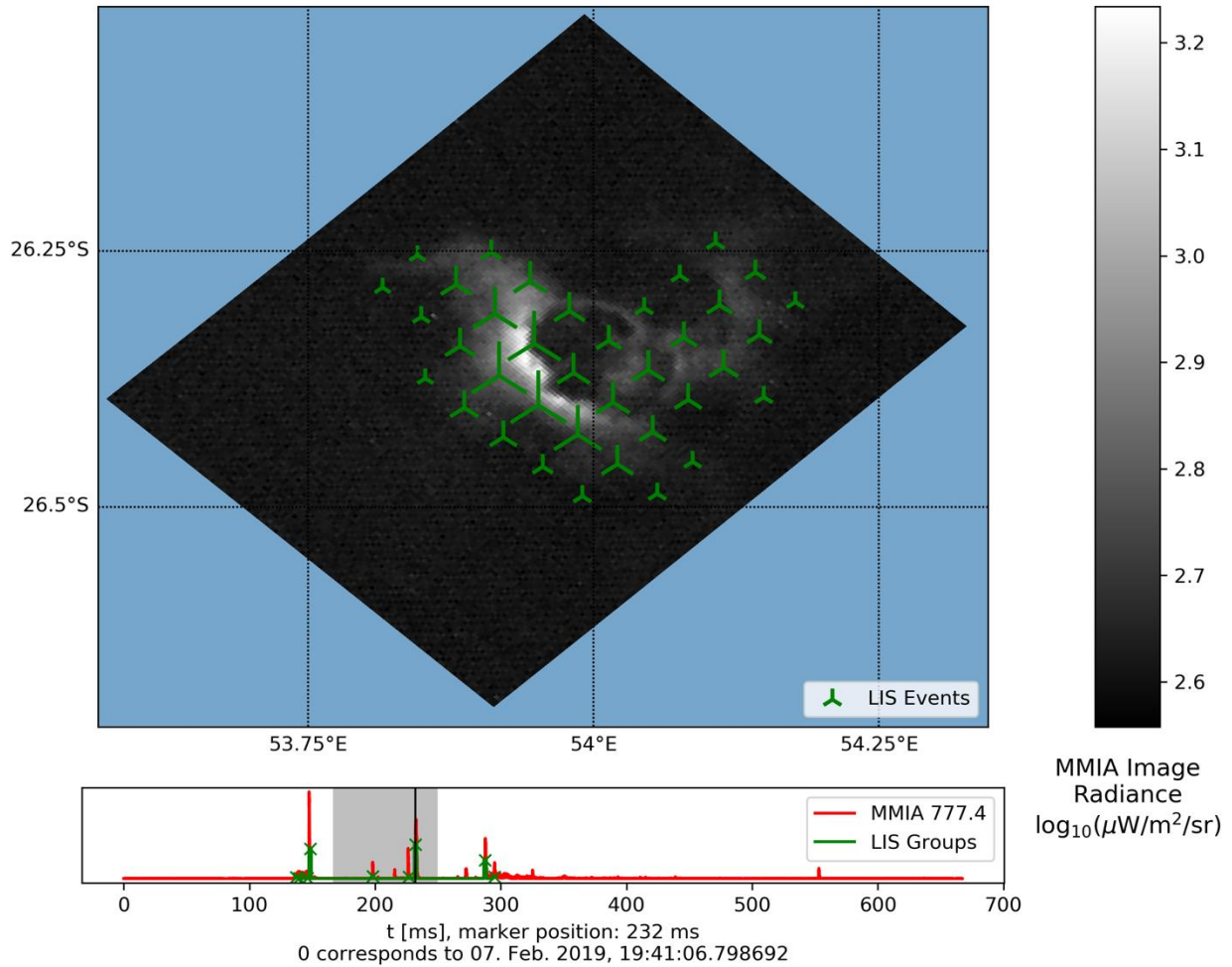


Figure 1.



Figure 2.

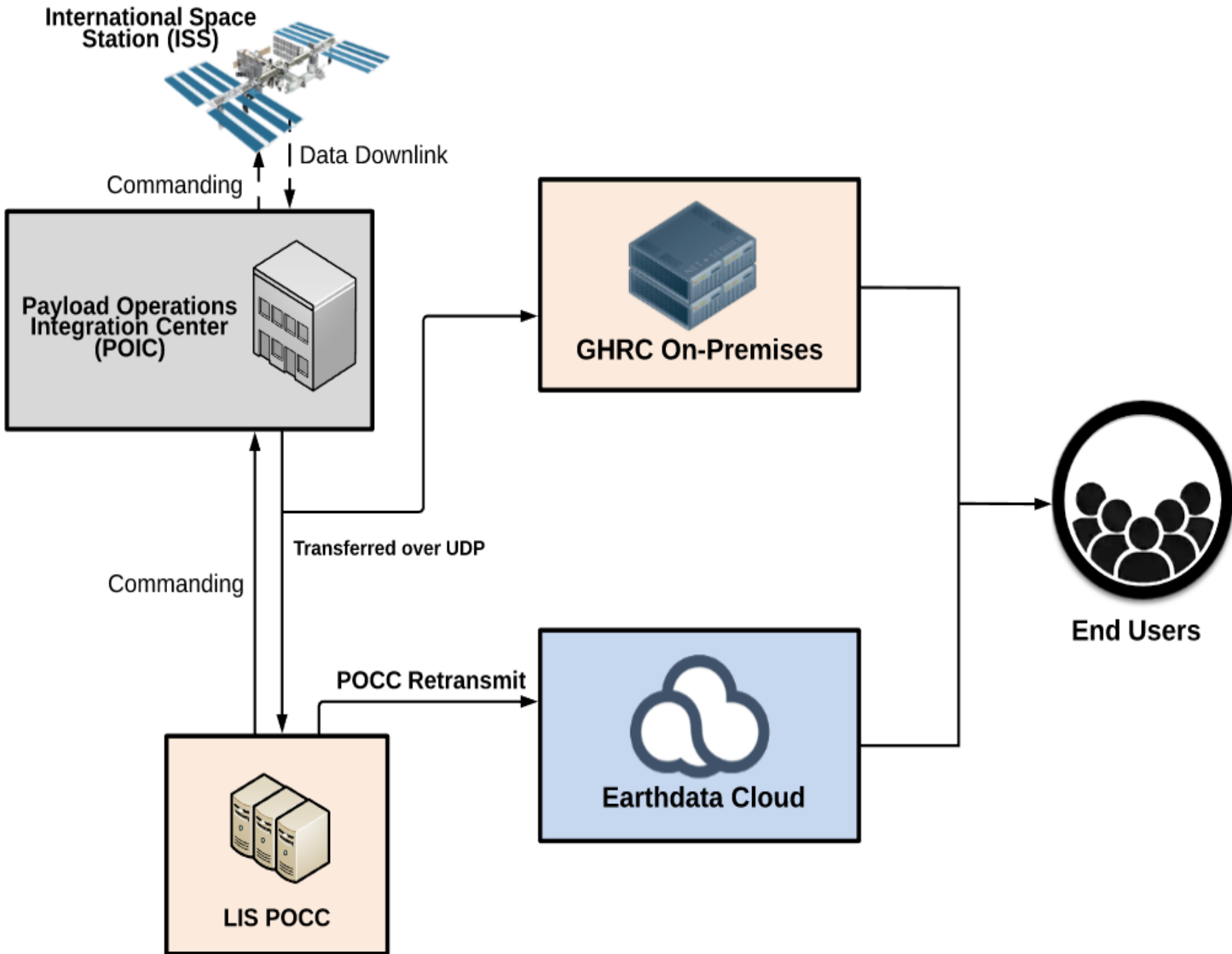
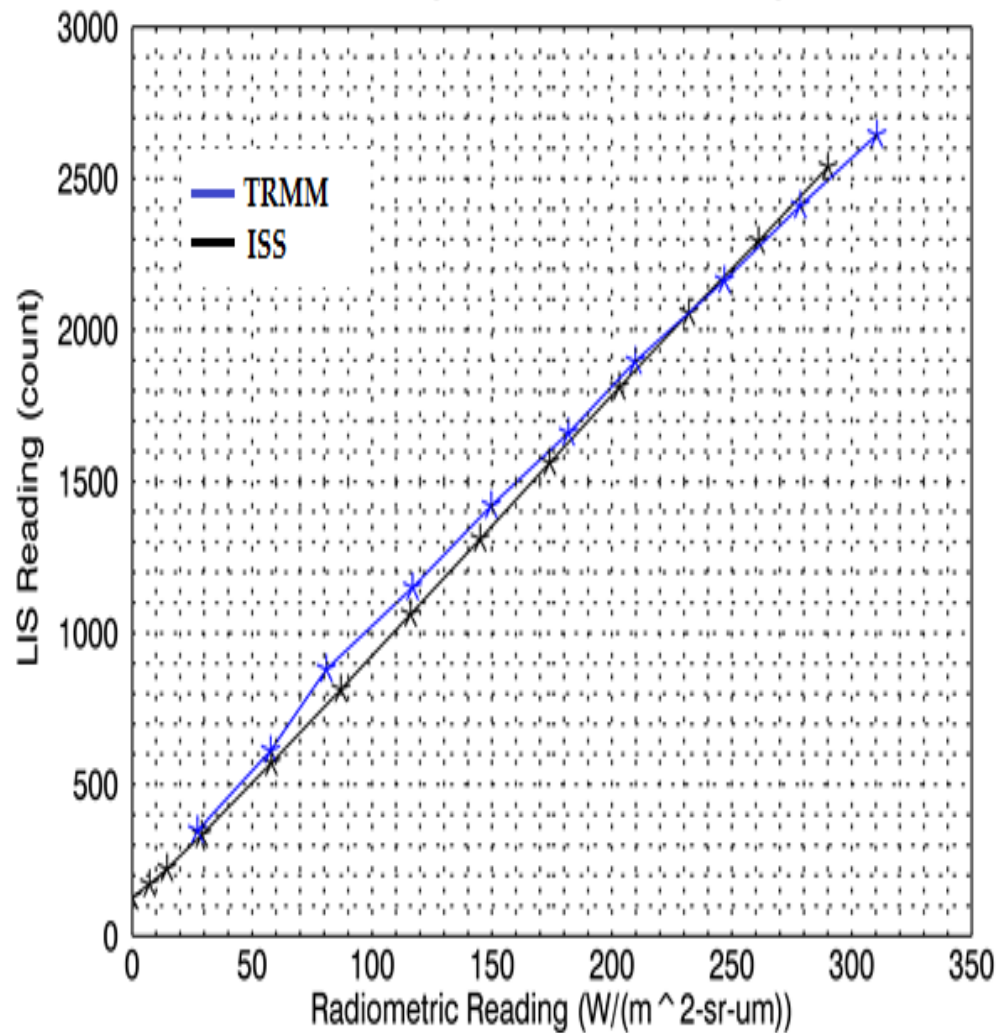
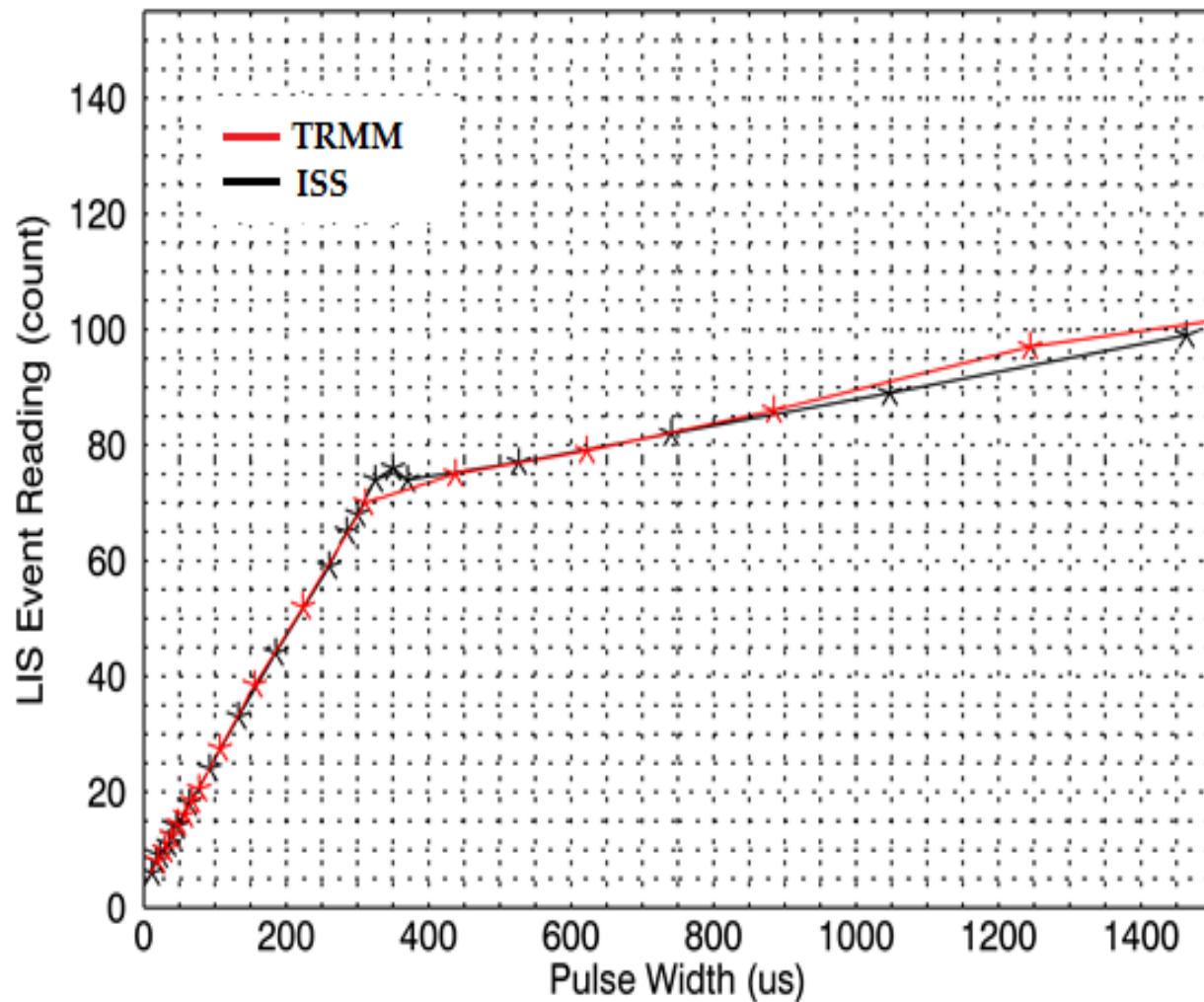


Figure 3.

### Static Response Test Comparison



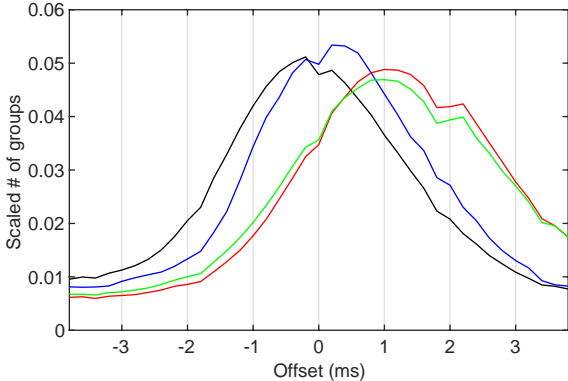
### Transient Response Test Comparison



**Figure 4.**

Temporal offset (reference time - LIS group time): 2017-03-01 to 2019-12-31

Peak<sub>EN</sub> = -0.2 ms; peak<sub>GLD</sub> = 0.2 ms; peak<sub>G16</sub> = 1 ms; peak<sub>G17</sub> = 1 ms



Distance offset: 2017-03-01 to 2019-12-31

Peak<sub>EN</sub> = 3 km; peak<sub>GLD</sub> = 3 km; peak<sub>G16</sub> = 2 km; peak<sub>G17</sub> = 2.5 km

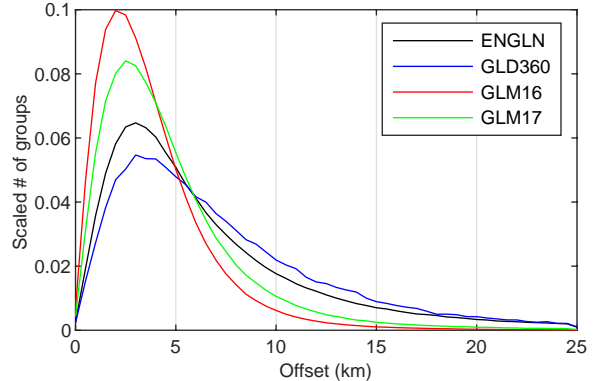
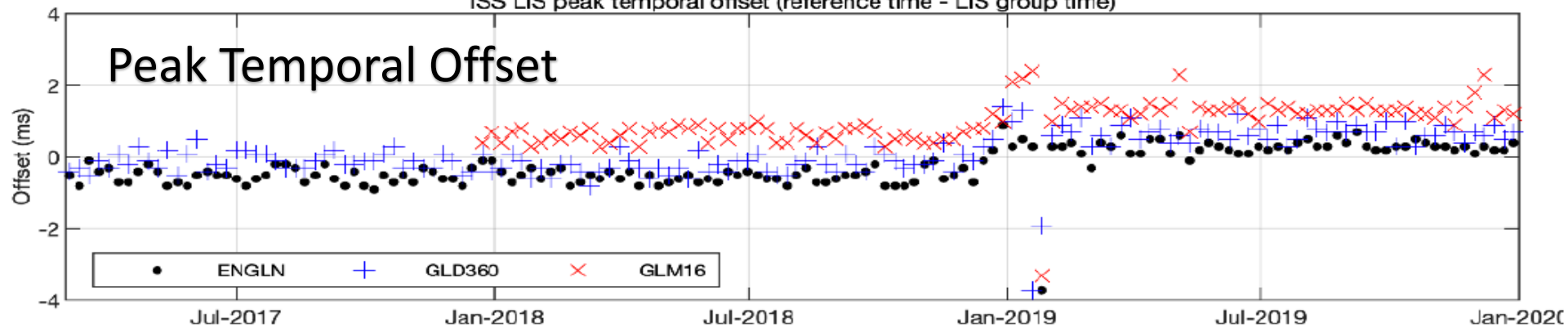
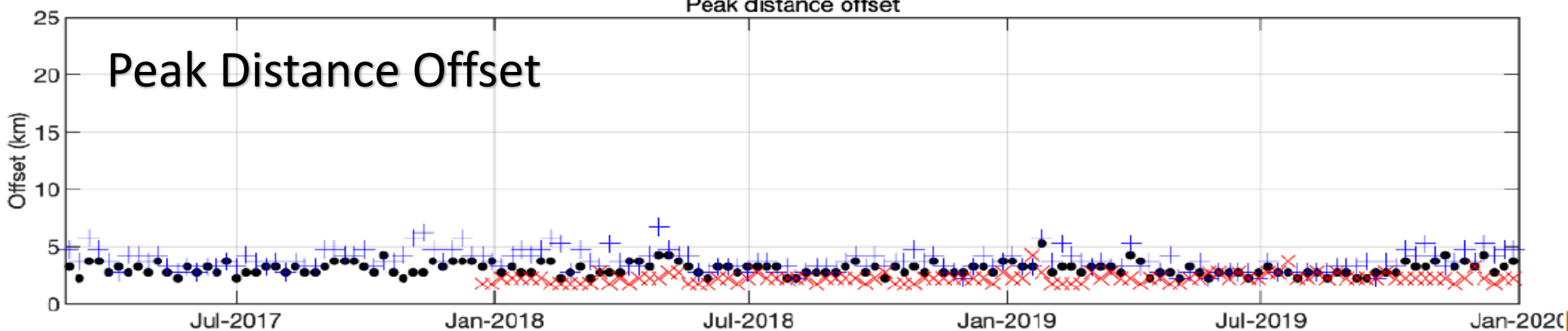


Figure 5.

ISS LIS peak temporal offset (reference time - LIS group time)



Peak distance offset



ISS LIS flash detection efficiency and false alarm rate

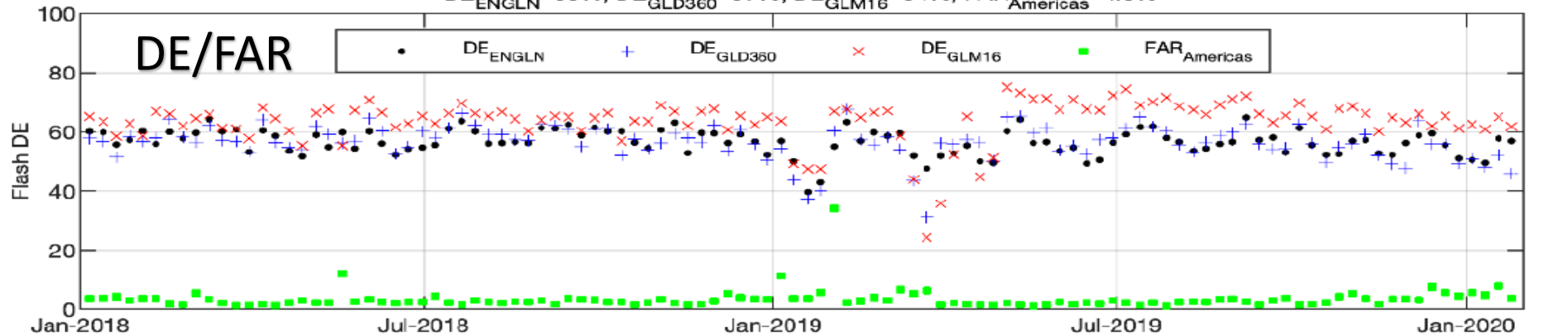
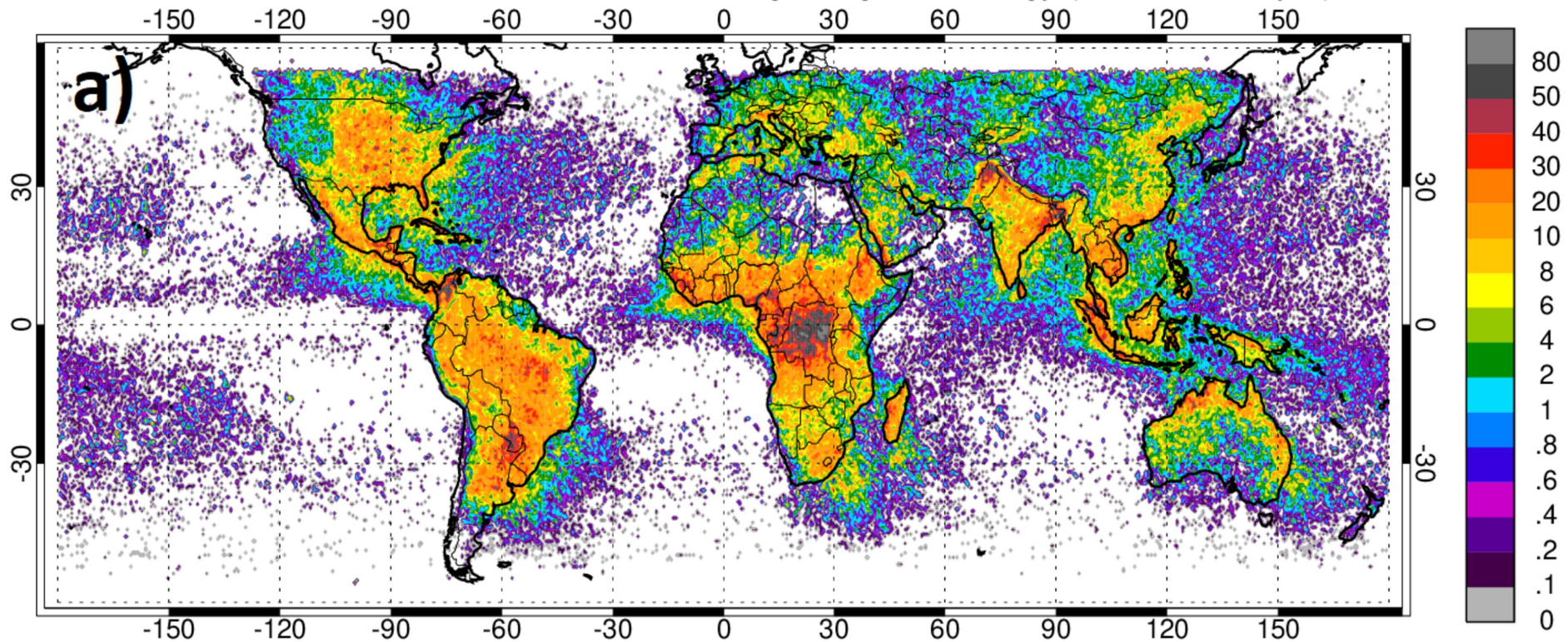
 $DE_{ENGLN}=56\%$ ;  $DE_{GLD360}=57\%$ ;  $DE_{GLM16}=64\%$ ;  $FAR_{Americas}=4.8\%$ 


Figure 6.

Mar 2017 - Feb 2020 0.5° ISS LIS Lightning Climatology (Flashes km<sup>-2</sup> yr<sup>-1</sup>)



Sep 2001 - Dec 2014 0.5° TRMM LIS Lightning Climatology (Flashes km<sup>-2</sup> yr<sup>-1</sup>)

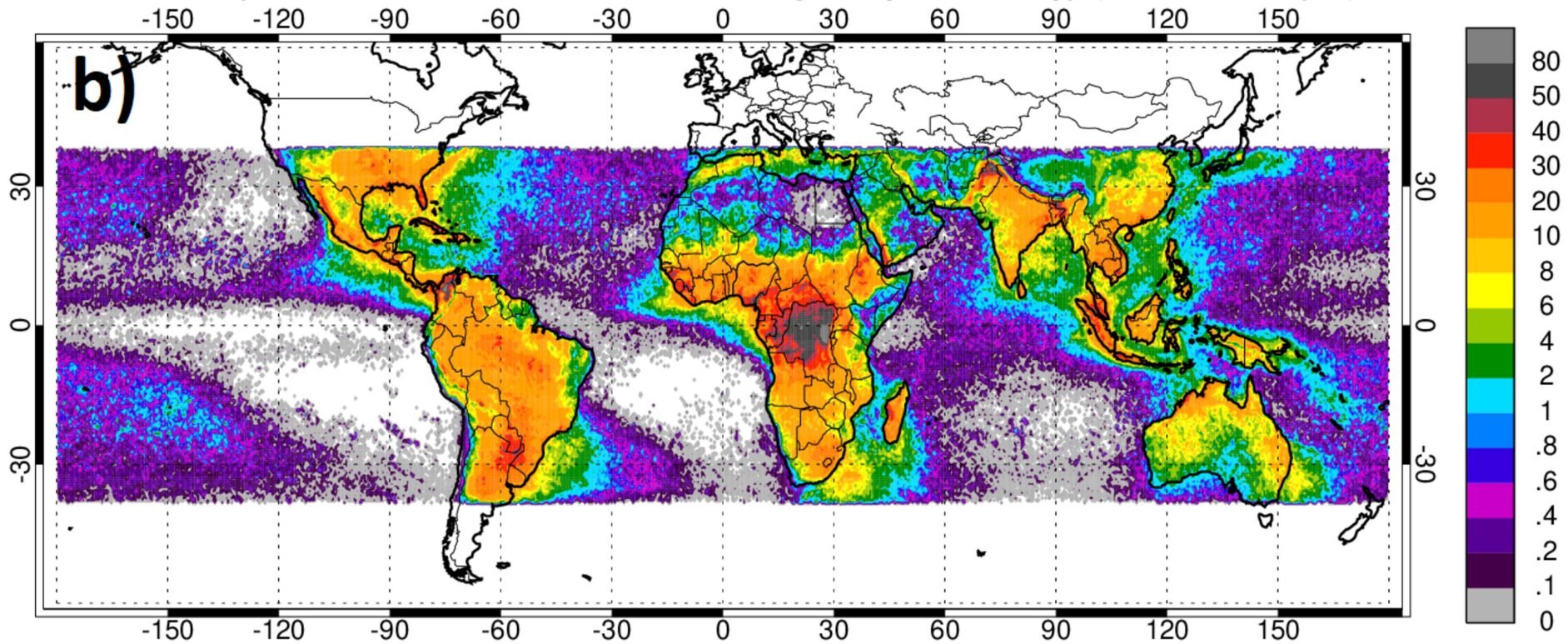


Figure 7.

# Monthly TRMM and ISS LIS Flash Rate

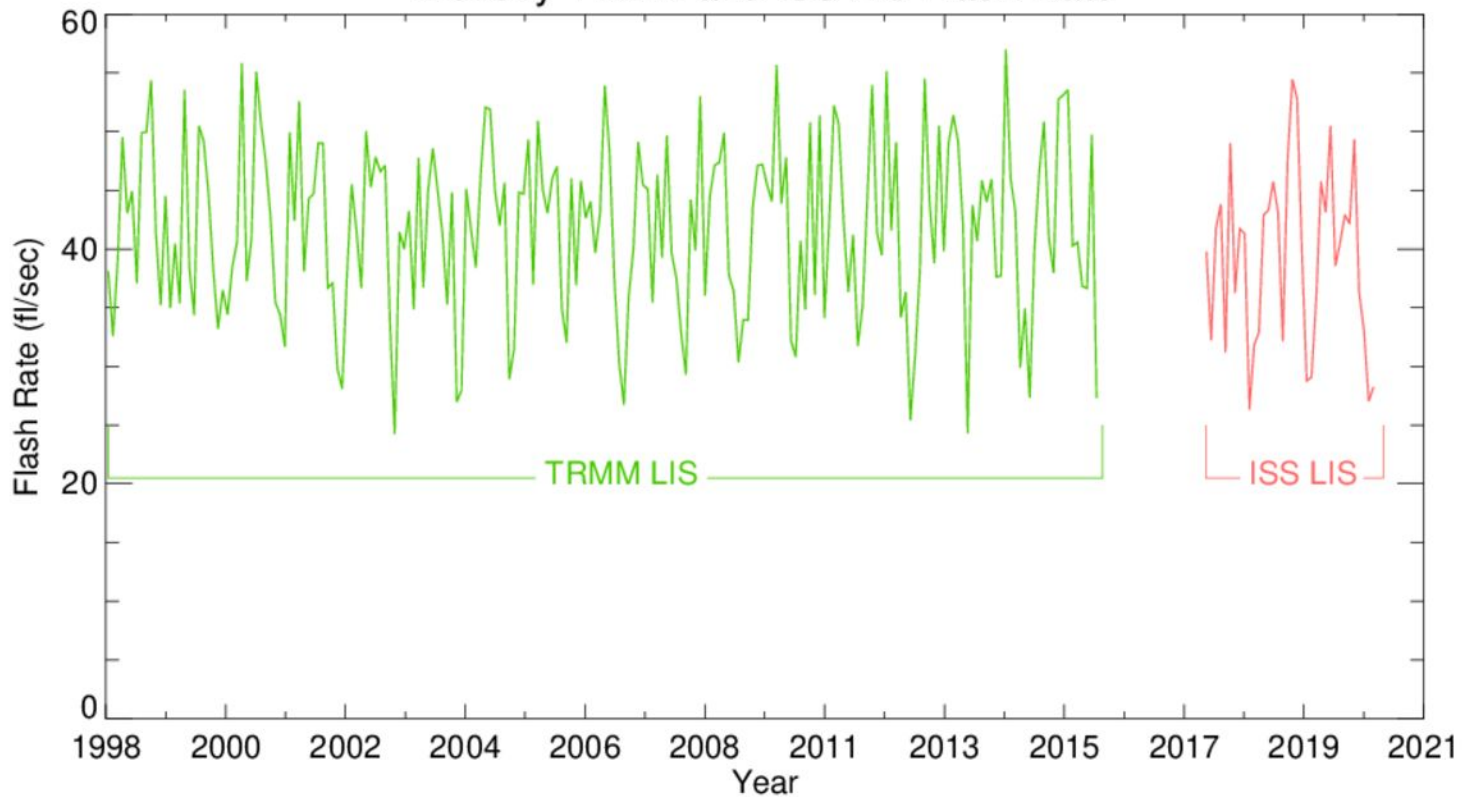
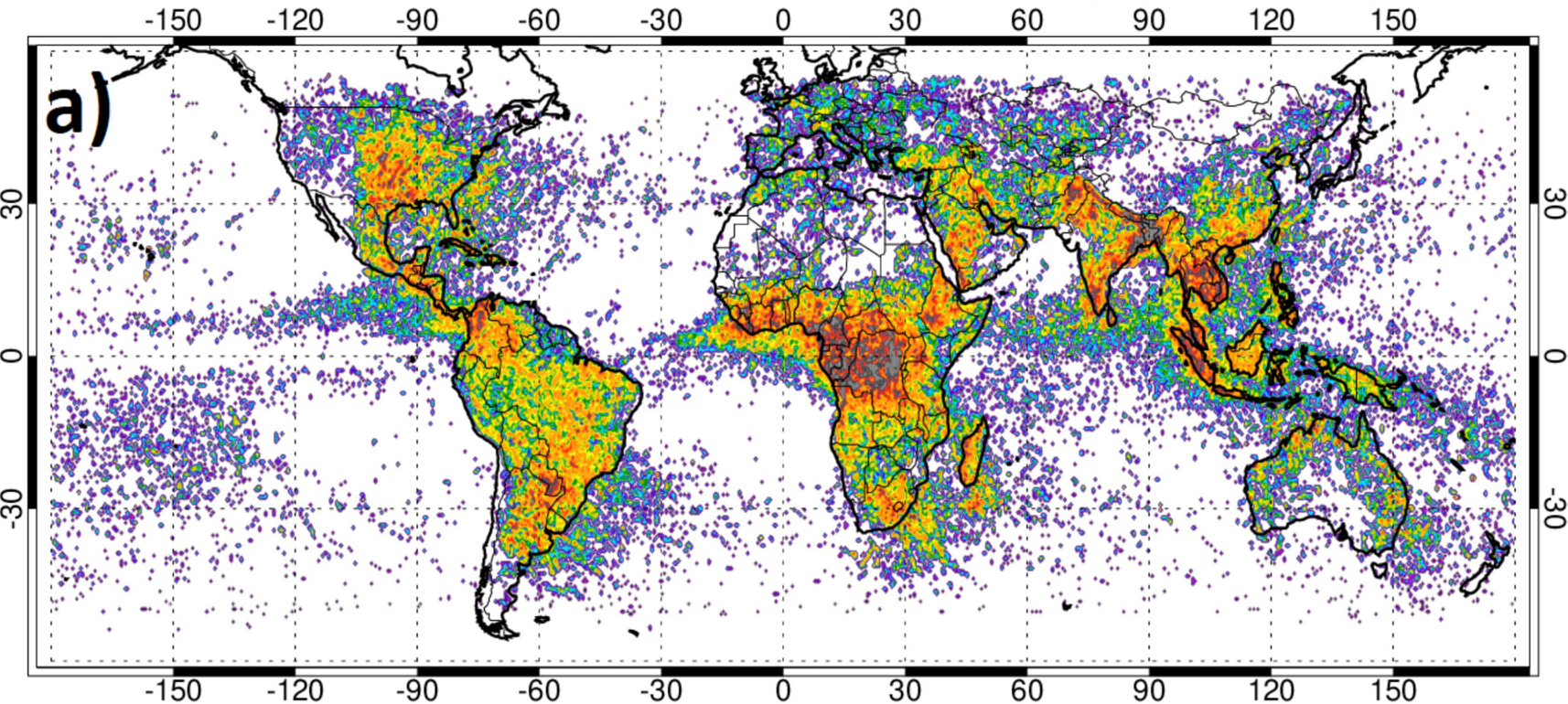
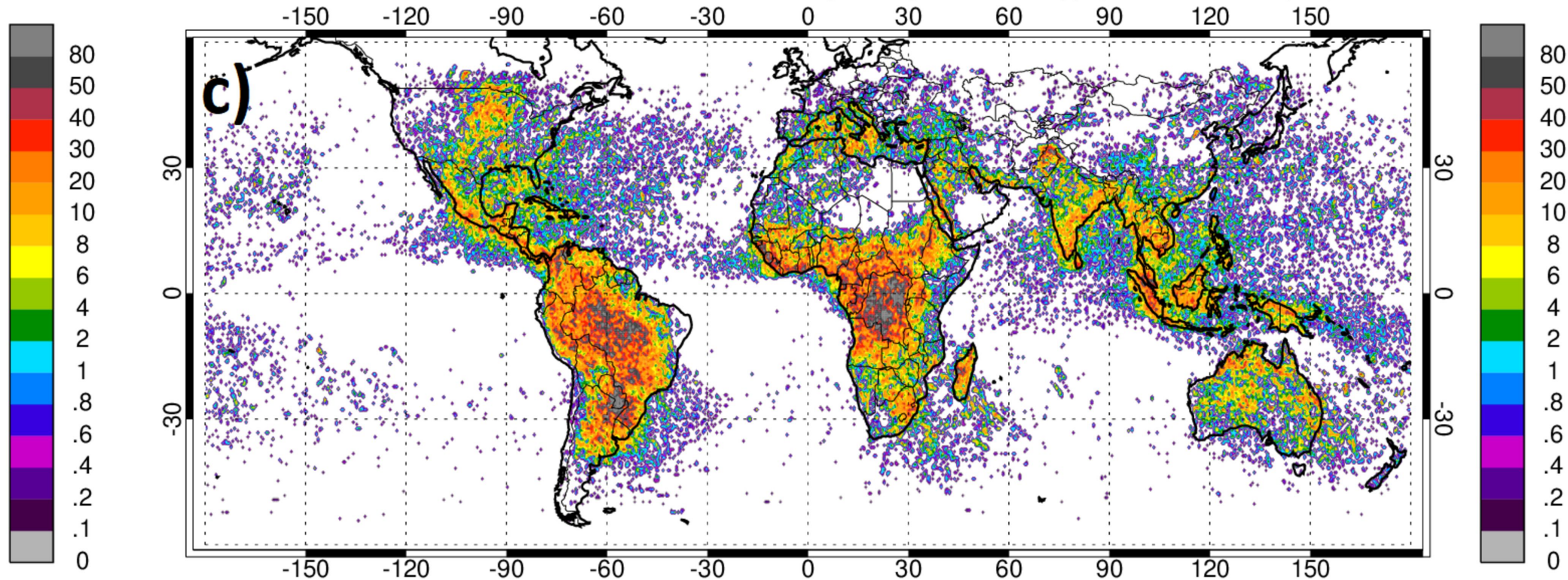


Figure 8.

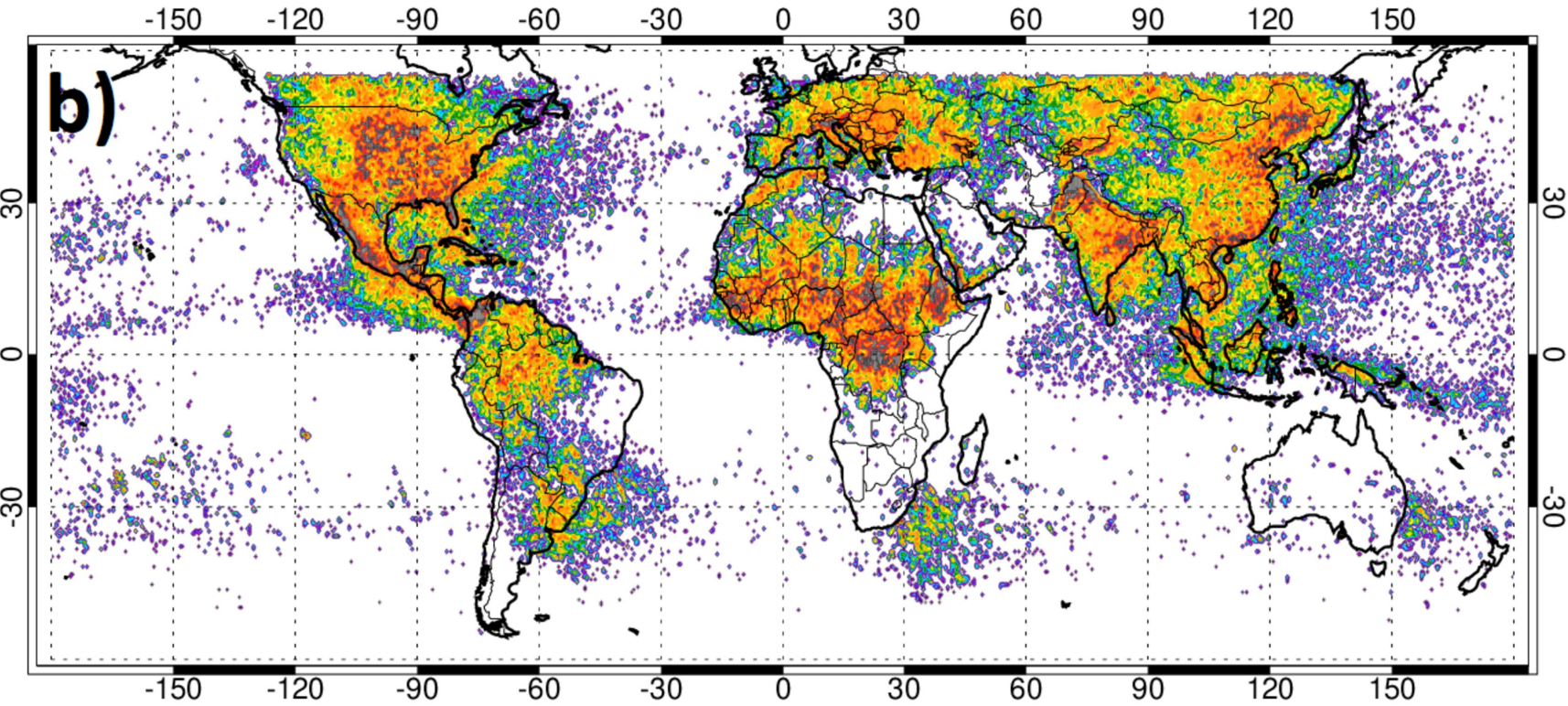
MAM 2017 - 2019 0.5° ISS LIS Lightning Climatology (Flashes km<sup>-2</sup> yr<sup>-1</sup>)



SON 2017 - 2019 0.5° ISS LIS Lightning Climatology (Flashes km<sup>-2</sup> yr<sup>-1</sup>)



JJA 2017 - 2019 0.5° ISS LIS Lightning Climatology (Flashes km<sup>-2</sup> yr<sup>-1</sup>)



DJF 2017 - 2020 0.5° ISS LIS Lightning Climatology (Flashes km<sup>-2</sup> yr<sup>-1</sup>)

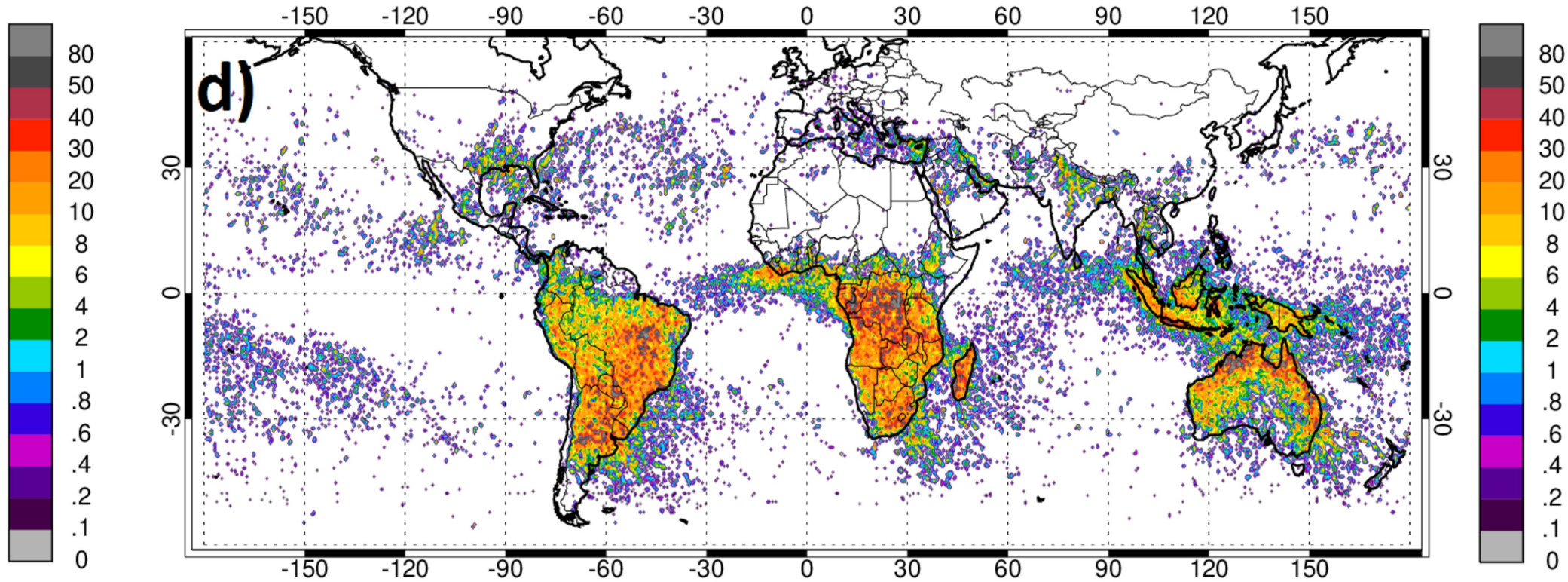
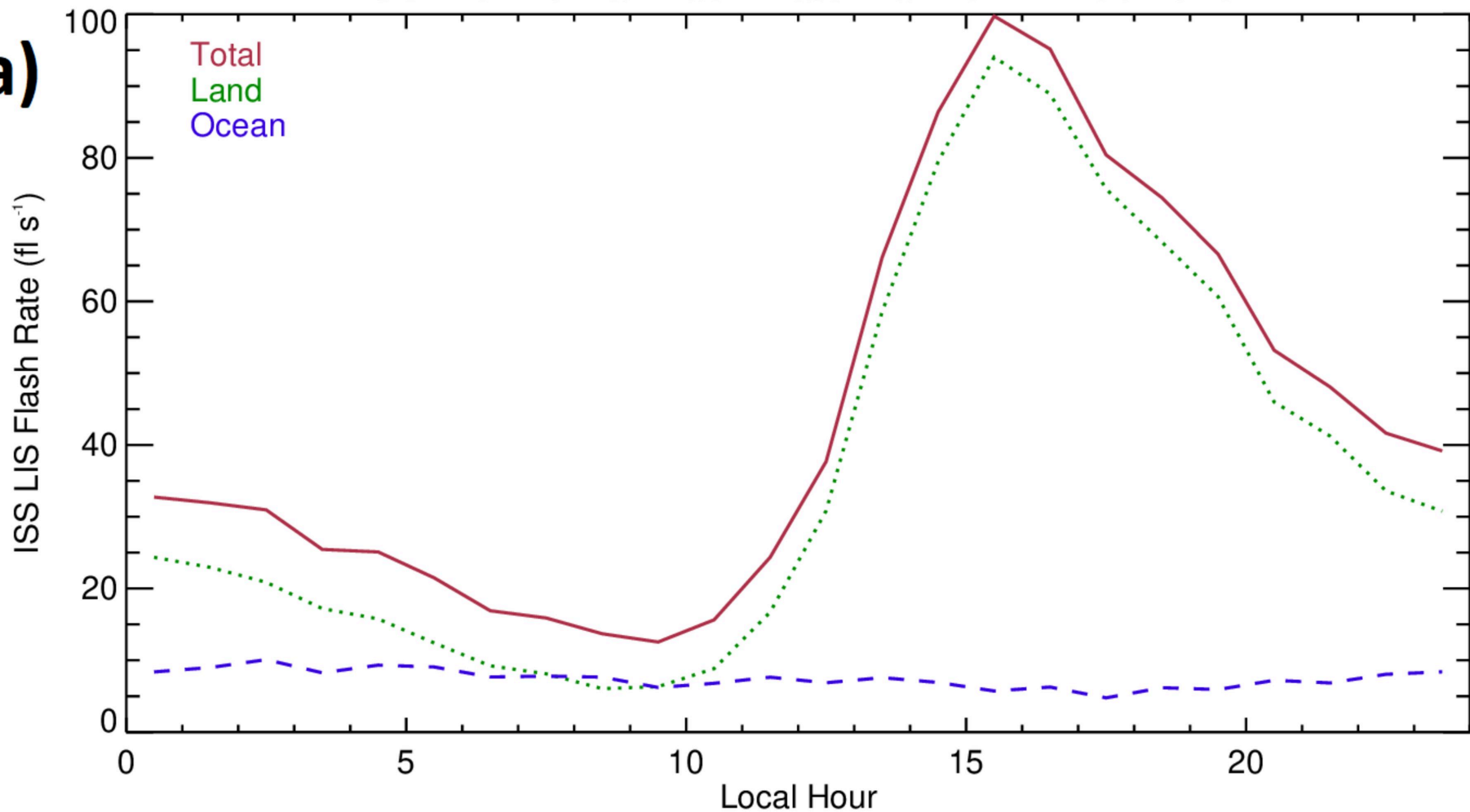


Figure 9.

ISS LIS Diurnal Flash Rate Mar 2017 - Feb 2020

**a)**

ISS LIS UTC Flash Rate Mar 2017 - Feb 2020

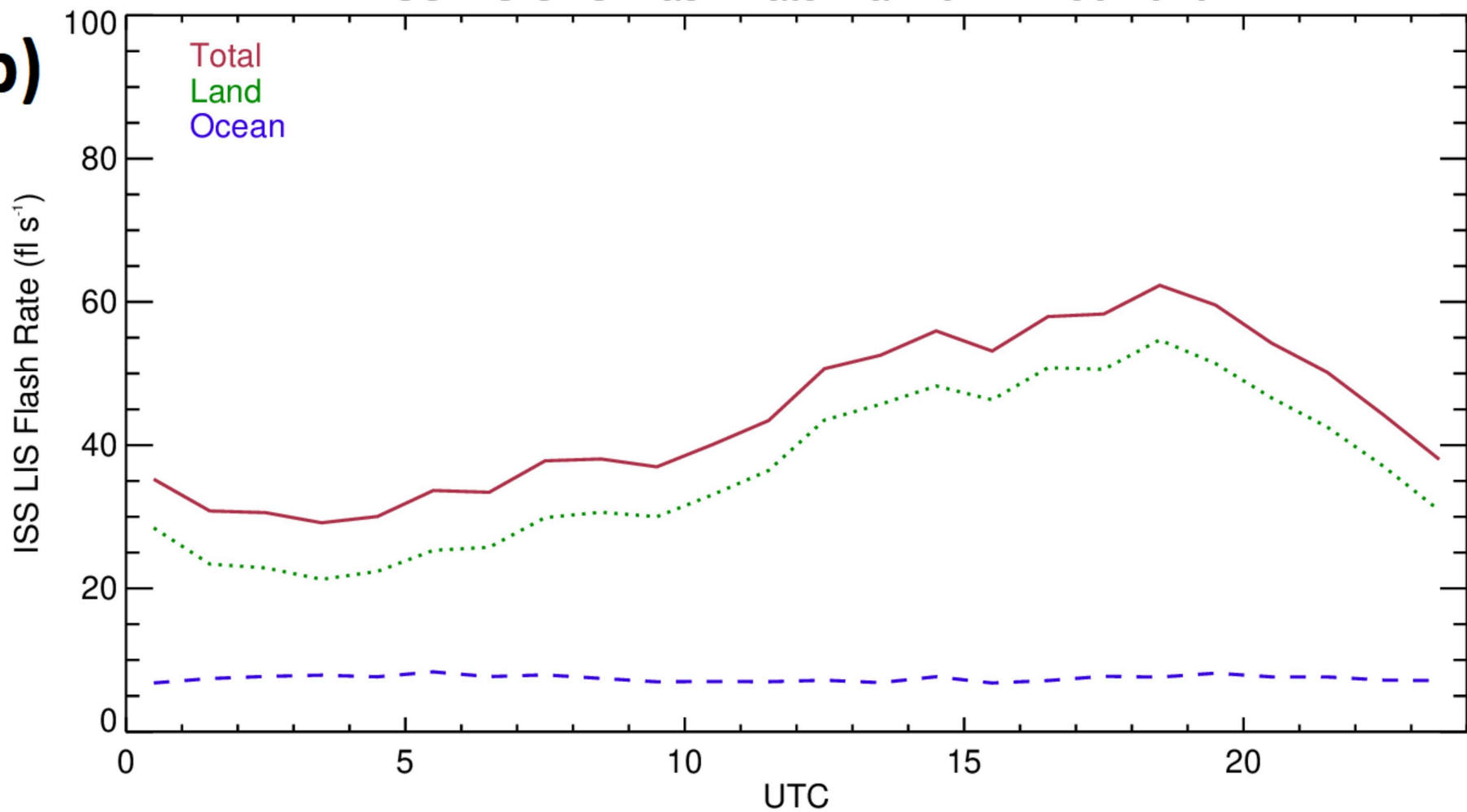
**b)**

Figure 10.

GLM-16 flash DE with respect to reference data  
Matching window = 200 ms, 50 km; 2018-01-01 to 2019-12-31

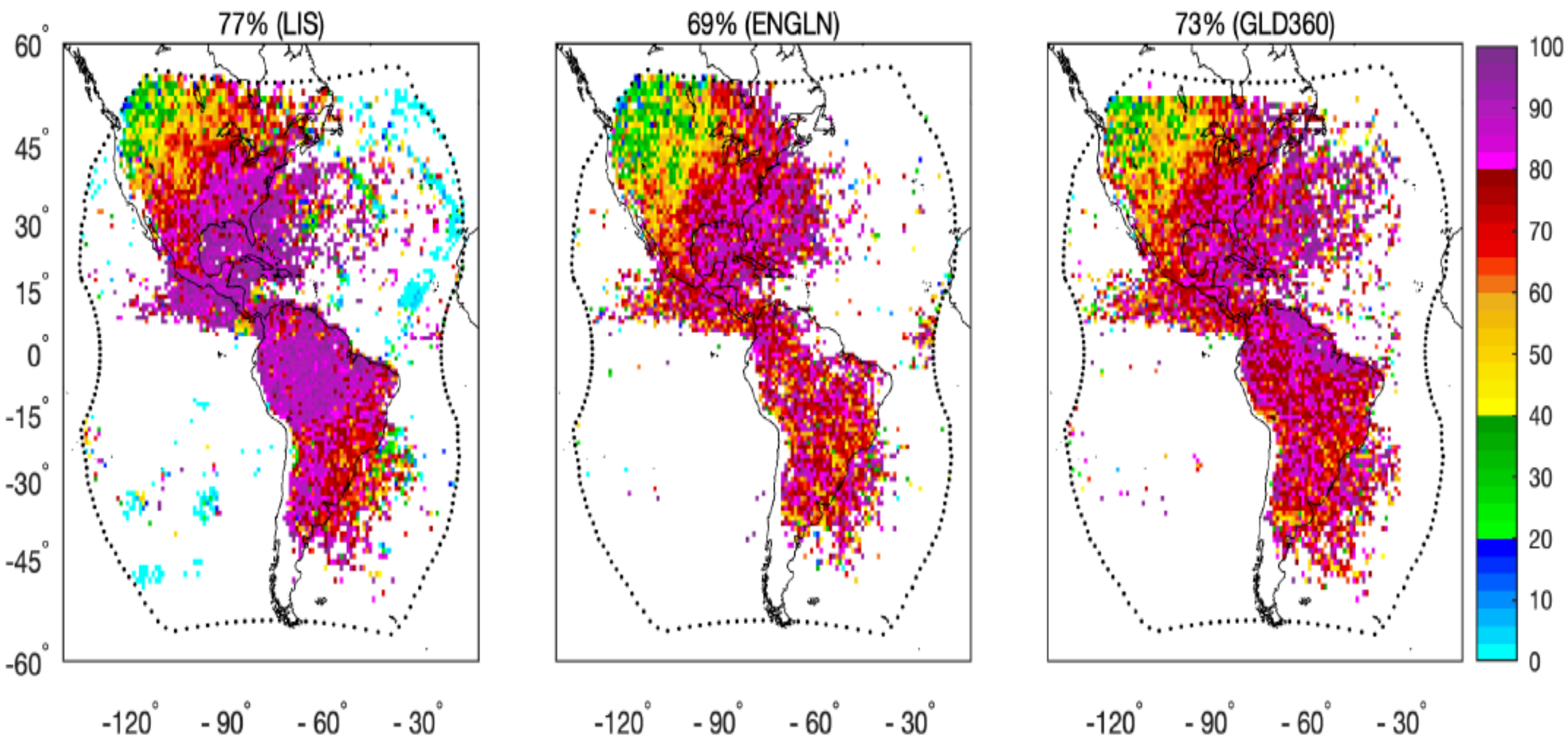


Figure 11.

## Risk Analysis



0 100 200 Kilometers

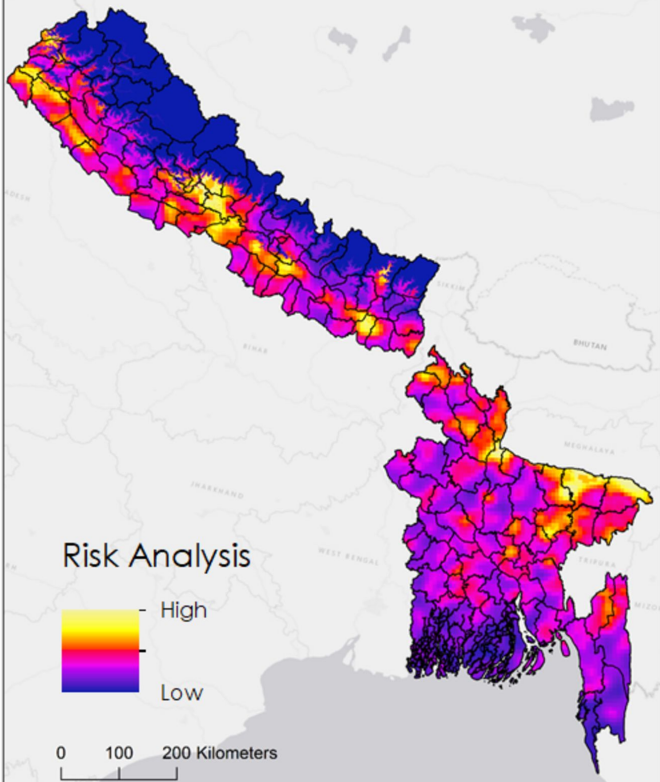


Figure 12.

